A subordinated advection model for uniform bedload transport from local to regional scales

Yong Zhang

1) University of Alabama, Tuscaloosa, AL, USA 2) Hohai University, Nanjing, China

Raleigh L. Martin

University of California, Los Angeles, CA, USA

Dong Chen

Chinese Academy of Sciences, Beijing, China

Boris Baeumer

University of Otago, Dunedin, New Zealand

Hongguang Sun

Hohai University, Nanjing, China

Li Chen

1) Desert Research Institute, NV, USA 2) Hohai University, China

---

Yong Zhang, 1) Department of Geological Sciences, University of Alabama, Tuscaloosa, AL 35487, USA. 2) Hohai University, Nanjing 210098, China.

Raleigh L. Martin, Department of Atmospheric and Oceanic Sciences, University of California,

Abstract. Sediment tracers moving as bedload can exhibit anomalous dispersion behavior deviating from Fickian diffusion. The presence of heavy-tailed resting time distributions and thin-tailed step length distributions motivate adoption of fractional-derivative models (FDMs) to describe sediment dispersion, but these models require many parameters that are difficult to quantify. Here, we propose a considerably simplified FDM for anomalous transport of uniformly sized grains along straight channels, the subordinated advection equation (SAE), which is based on the concept of time subordination. Unlike previous FDM models with time index γ between 0 and 1, our SAE model adopts a value of γ between 1 and 2. This γ describes random velocities deviating significantly from the mean velocity and models both long resting periods and relatively fast displacements. We show that the model

Los Angeles, CA 90095, USA.

Dong Chen, Key Laboratory of Water Cycle and Related Land Surface Processes, Institute of Geographic Sciences and Natural Resources Research, Chinese Academy of Sciences, Beijing, China.

Boris Baeumer, Department of Mathematics and Statistics, University of Otago, Dunedin, New Zealand.

Hongguang Sun, College of Mechanics and Materials, State Key Laboratory of Hydrology-Water Resources and Hydraulic Engineering, Hohai University, Nanjing 210098, China.

Li Chen, 1) Division of Hydrologic Sciences, Desert Research Institute, Las Vegas, NV 89119, USA. 2) Hohai University, Nanjing 210098, China.

quantifies the dynamics of four bedload transport experiments recorded in the literature. In addition to γ, SAE model parameters–velocity and capacity coefficient–are related to the mean and variance of particle velocities, respectively. Successful application of the SAE model also implies a universal probability density for the heavy-tailed waiting time distribution (with finite mean) and a relatively lighter tailed step length distribution for uniform bedload transport from local to regional scales.

1. Introduction

Quantifying transport along sediment beds is important for stream restoration and river morphology [*Shields et al.*, 2003; *Lenzi et al.*, 2006; *Sear*, 2006]. To quantify the intermittent displacement of sediment particles, stochastic models have been developed extensively, after the pioneering work of *Einstein* [1937]. Regardless of the mode of transport in rolling, saltating, or sliding, bedload sediment particles typically move in a series of discrete steps consisting of alternate transportation and storage [*Sayre and Hubbell*, 1965]. The complex bedload transport process therefore can be simplified as a random walk in stochastic models, where the core challenge lies in determining the probability density functions (PDFs) for the step lengths during each movement and the resting times separating two subsequent jumps [*Einstein*, 1937; *Bradley et al.*, 2010]. As a result of these stochastic step lengths and resting times, sediment particles disperse through time, and a major research challenge lies in connecting this stochastic behavior of individual particles to overall dispersion of the plume of sediment tracers [*Ganti et al.*, 2010].

Einstein [1937] proposed a Poisson model to interpret the random nature of sediment dynamics. Einstein's model assumes an exponential PDF for both travel distances and resting times, producing Fickian diffusion. This model captures thin-tailed bedload transport, but misses heavy-tailed dynamics, commonly observed in sediment tracer studies [*e.g., Bradley et al.*, 2010]. Here a heavy tail means that the probability density falls off with the step length (or resting time) as a negative power law (following the definition in *Hill et al.* [2010]), while a thin tail means that the probability declines faster than a power law function.

Fractional-derivative models (FDM) [*Metzler and Klafter*, 2000; *Meerschaert and Sikorskii*, 2012] have been proposed as promising alternatives to Fickian transport models. Derivatives of fractional order can effectively capture heavy-tailed fast jumps (where the probability density for fast displacement of random walkers declines as slowly as a power law function), causing researchers to apply the fractional advection-dispersion equation (fADE) to sediment transport [*Stark et al.*, 2009; *Schumer et al.*, 2009; *Ganti et al.*, 2010]. *Bradley et al.* [2010] first applied a space fADE model to sediment dispersion observed in the field. In their model, each jump time is separated into a random flight and resting time for mobile and immobile phases, respectively, of particle motion. The fADE model describes evolution of the sediment concentration probability density, P $[ML^{-1}]$, with "operational time", τ. The operational time describes the equivalent amount of time that a particle would have spent in motion had it traveled at the mean particle velocity. The fADE model can be formulated as [*Bradley et al.*, 2010]:

$$\frac{\partial P(x,\tau)}{\partial \tau} = -\bar{u}_\tau \frac{\partial P(x,\tau)}{\partial x} + \mathcal{D}\frac{\partial^\alpha P(x,\tau)}{\partial x^\alpha} \ , \tag{1}$$

where $\bar{u}_\tau$ $[LT^{-1}]$ is the mean mobile particle velocity; $\mathcal{D}$ $[L^\alpha T^{-1}]$ denotes a fractional dispersion coefficient; and $1 < \alpha < 2$ [dimensionless] is the order of the Riemann-Liouville fractional derivative. Values of α in this range indicate "super-diffusion," i.e., the variance of tracer particle displacement increases faster than linearly in time. Model 1 captures the heavy-tailed leading edge of particle displacement in the case of a wide distribution of particle sizes, such as observed by *Hill et al.* [2010].

The space fADE model 1 can then be generalized to account for the natural truncation of particle jump lengths and resting times [*Zhang et al.*, 2012]:

$$\begin{aligned}\frac{\partial P(x,t)}{\partial t} + \beta e^{-\lambda_t t}\frac{\partial^\gamma [e^{\lambda_t t}P(x,t)]}{\partial t^\gamma} - \beta(\lambda_t)^\gamma P(x,t) = -v\frac{\partial P(x,t)}{\partial x} \\ + D\left\{e^{-\lambda_x x}\frac{\partial^\alpha [e^{\lambda_x x}P(x,t)]}{\partial x^\alpha} - \alpha(\lambda_x)^{\alpha-1}\frac{\partial P(x,t)}{\partial x} - (\lambda_x)^\alpha P(x,t)\right\},\end{aligned} \tag{2}$$

where β $[T^{\gamma-1}]$ is the capacity coefficient; λ_t $[T^{-1}]$ and λ_x $[L^{-1}]$ are the truncation parameters in time and space, respectively; γ [dimensionless] $(0 < \gamma < 1)$ is the time index which defines the order of the fractional derivative; and v $[LT^{-1}]$ and D $[L^\alpha T^{-1}]$ are the effective velocity and dispersion coefficient, respectively. The time fractional derivative term on the left hand side of eqn. 2 captures a time nonlocal process due to the trapping of sediment, while the space fractional derivative term on the right hand side describes a space nonlocal process due to very long particle flights. The spatiotemporal fADE 2 can capture a wide spectrum of sediment dynamics [*Zhang et al.*, 2012].

Two knowledge gaps in these promising fractional-derivative models motivated this study. First, the above FDMs are not trivial in their application. The dispersion coefficient is usually difficult to predict, and the combination of space and time nonlocal processes in eqn. 2 complicates practical application by requiring too many parameters whose physical basis is not yet fully understood. Is it possible to develop a simple model with fewer parameters to capture uniform bedload transport across scales? Do space and time nonlocality exist simultaneously for all sediment transport? Second, it remains unclear whether there are universal probability densities for step lengths and resting times that properly capture a typical bedload transport process. This knowledge gap might be filled after extensive applications of the FDMs. However, to the best of our knowledge, the

above fADE models have only been applied to a few studies of observed bedload transport [*Bradley et al.*, 2010; *Zhang et al.*, 2012].

This study aims to develop and apply a simple physically-based model to further explore the random nature of bedload sediment dynamics, especially the probability densities of sediment step lengths and resting times. To reach this goal, the rest of the paper is organized as follows. In Section 2, the physics of uniform sediment transport are discussed. In Section 3, a physical model based on subordination is developed to capture the dynamics of uniform sediment transport, given the statistics of sediment transport analyzed in Section 2. In Section 4, the new model and its solver are applied to capture bedload transport documented in the literature from local to regional scales. In Section 5, we discuss the approximation of model parameters and possible extensions of the stochastic model. The above bedload transport models–Einstein's Poisson model and the fADE models 1 and 2–are also discussed and evaluated for comparison in Sections 4 and 5. Conclusions are finally drawn in Section 6. Mathematical derivation of the model, following the pioneering work in *Meerschaert et al.* [2010], is shown in Appendix A for interested readers.

2. Physical basis

2.1. PDFs of sediment step lengths and resting times

Many studies have found that the PDF of sediment step lengths can exhibit a much lighter tail than the resting time PDF. Step lengths for uniform bedload tracers typically exhibit a distribution thinner than power-law in gravel-bed rivers and flumes. For example, *Schmidt and Ergenzinger* [1992] found that the distribution of step lengths can be approximated by an exponential function, after conducting radio tracer experiments in a step-pool mountain river. *Hodge et al.* [2011] found that the bedload sediment

transport distances in bedrock or alluvial rivers follow gamma distributions. Relatively thin-tailed step length distributions with convergent first moments (including log-normal and chi-squared distributions) were also found by other studies [*Chang and Yen*, 2002; *Niño et al.*, 2003; *Marion et al.*, 2008; *Houssais and Lajeunesse*, 2012; among many others]. Several other researchers have also argued that the particle step lengths should have a power-law distribution with divergent mean values, considering 1) the strong randomness associated with various factors affecting particle movement especially at large scales [*Stark et al.*, 2009; *Ganti et al.*, 2010; *Bradley et al.*, 2010] and 2) the wide distribution of particles sizes for natural bedload [*Hill et al.*, 2010]. This study considers a uniform grain size, and we will test whether the corresponding step length PDF has a thin tail using laboratory and field observations.

In contrast to the typically thin-tailed distributions of step lengths, heavy-tailed resting times for bedload particles are well documented. For example, *Haschenburger and Wilcock* [2003] found that the random resting period for sediments can be very long, with an upper limit depending on the scaled discharge. *Cudden and Hoey* [2003] identified anomalous diffusion in bedload transport along a gravel-bed braided stream due to the strong influence of long resting periods on sediment dynamics. *Ferguson et al.* [1996] observed strongly right-skewed travel distances for tracer pebbles along a 2.5 km gravel-bed reach, probably due to the strong impact of trapping. *Lajeunesse et al.* [2010] visualized the trajectories of entrained grains above a flat sediment bed of uniform grain size and identified the strong influence of immobile phases on bedload transport. *Martin et al.* [2012] traced the motion of individual gravels under near-threshold intermittent bedload transport through a flume, and they found an exponential distribution of particle flight

lengths and power-law distributed rest durations, which may be related to the return time distribution for bed scour.

We will account for the different distributions of step lengths and waiting times by developing a simple physical model for transport. In particular, in the next section we will quantify both thin- and heavy-tailed bedload transport processes by proposing a general physical model where the operational time distribution has a finite mean.

It is also noteworthy that many factors can affect sediment transport and the corresponding PDFs for sediment dynamics, including, for example, bed topography and elevation [*Bennett and Bridge*, 1995; *Dancey et al.*, 2002; *Wong et al.*, 2007], channel morphology [*Pyrce and Ashmore*, 2003a, 2003b; *Strom et al.*, 2004; *Johnson and Whipple*, 2007; *Eaton and Church*, 2009], flow conditions [*Lee et al.*, 2004; *Pecking*, 2009; *Fraccarollo and Rosatti*, 2009; *Bombar et al.*, 2011; *Tritthart et al.*, 2011], and sediment input [*Madej et al.*, 2009]. The spatiotemporal interaction and variability of these factors at various scales can result in complex dynamics of bedload transport. In addition, the wide range of grain sizes composing the bed can also complicate bedload transport [e.g., *Wilcock*, 1992; *Park and Klingeman*, 1982; *Houssais and Lajeunesse*, 2012]. To minimize complicating factors, this study focuses on the stochastic modeling of sediment transport along a relatively straight channel bed where the tracer particles have relatively uniform size. The extension to mixed-size beds will be briefly discussed in section 5. Various scales for bedload transport are also considered in model applications, since the anomalous bedload dynamics may depend on the scale of transport [*Nikora et al.*, 2002].

2.2. Major properties of the continuous time random walk process

Here we simplify the bedload transport process as a continuous time random walk (CTRW) with two specific properties. The CTRW describes a discrete stochastic process with alternating jumps and rests. First, our specific CTRW model allows continuous movement of tracer particles. A sediment particle can move continuously before becoming trapped in the bed. Second, waiting times of the CTRW are assumed to have finite mean and infinite variance (i.e., one of the CTRW processes that was well studied by *Baeumer and Meerschaert* [2007] and *Meerschaert et al.* [2010]), to characterize the heavy-tailed PDF of sediment resting times. In other words, the extreme events for long resting times are considered by this CTRW process. This assumption therefore provides an alternative of model 2, which truncates the long waiting time to obtain a waiting time distribution with finite mean [*Zhang et al.*, 2012]. As will be shown below, this assumption also allows for estimation of the mean velocity in the CTRW process. We will check this assumption by applying the resultant physical model in quantifying sediment transport in section 4.

3. Theoretical derivation

3.1. Model development

A mathematical method called subordination [*Baeumer et al.*, 2001] is used to build a transport model that can incorporate all of the physical principles discussed in section 2. In this method, the physical time is randomized to represent the operational time experienced by an individual tracer particle [*Baeumer et al.*, 2001; *Harman et al.*, 2010]. Following the method in *Meerschaert et al.* [2010], the subordinator corresponding to a γ-stable waiting time process with index $1 < \gamma \leq 2$ satisfies the governing equation for

the density of operational time, $h(\tau, t)$:

$$-\beta \frac{\partial^\gamma h(\tau,t)}{\partial t^\gamma} + \frac{\partial h(\tau,t)}{\partial t} = -\frac{\partial h(\tau,t)}{\partial \tau}; \quad h(\tau,0) = \delta(\tau) \tag{3}$$

where the operator $\partial^\gamma/\partial t^\gamma$ denotes a first degree fractional Caputo derivative, i.e., $\frac{\partial^\gamma}{\partial t^\gamma} = \frac{\partial}{\partial t} D_t^{\gamma-1}$, and $D_t^{\gamma-1}$ is a Caputo-type fractional derivative [*Miller and Ross*, 1993]. This operator models power-law waiting times [*Baeumer and Meerschaert*, 2007]. Here the subordinator means that, if the time (denoted as τ) of the nth particle jump is well approximated by a γ-stable process with shape parameter β, then the density giving the number of jumps by time t is well approximated by the subordinator $\tau \mapsto h(\tau, t)$. Based on the time subordination described by eqn. 3 and given any linear spatial operator A modeling transport and/or dispersion, such as $A = -\nabla v + \nabla D \nabla$ (where the symbol "∇" is the Laplace operator), the subordinated process for sediment transport has a concentration density $P(x, t)$ that solves (see Appendix A for a brief derivation):

$$-\beta \frac{\partial^\gamma P(x,t)}{\partial t^\gamma} + \frac{\partial P(x,t)}{\partial t} = AP(x,t); \quad P(x,0) = P_0(x). \tag{4}$$

In one dimension, deviation from the mean velocity can mostly be captured by the variation in time spent in the substrate [*Harman et al.*, 2010]. Hence the most parsimonious model in this case (which is a subordinated advection equation, or SAE) is:

$$-\beta \frac{\partial^\gamma P(x,t)}{\partial t^\gamma} + \frac{\partial P(x,t)}{\partial t} = -v \frac{\partial}{\partial x} P(x,t); \quad P(x,0) = P_0(x). \tag{5}$$

When $\gamma \to 2$, solution of eqn. 5 is an inverse Gaussian PDF [*Kumar et al.*, 2011].

We note that our definitions of number density and average particle velocity do not incorporate the entire bedload transport active layer but only include the population of deployed tracers. In addition, model 5 is the governing equation for the scaling limit in time of an uncoupled CTRW with finite mean waiting times and continuous jumps

[*Meerschaert et al.*, 2010], and therefore it captures the major properties of a CTRW process described in section 2.2. Unlike previous fADE models 1 and 2, our model 5 does not explicitly define dispersion; instead, deviations from mean velocity are captured by the subordination operator.

3.2. Possible definition of model parameters

Several parameters are needed to develop the physical model. First, the average travel velocity of sediment particles, which can be approximated as the ratio of the average single step length to the average single jump time (flight plus rest), can be used to represent the constant velocity (denoted as v herein) of sediment transport. Velocity v should be functionally equivalent to the average particle velocity v_r defined by *Einstein* [1937]. Second, parameters γ and β relate true "clock" times to operational times, and describe respectively the scaling and shape of the operational time distribution. We further explore the physical meaning of these parameters later in this paper.

3.3. Numerical experiments

The SAE model 5 can be approximated by the Lagrangian solver [*Meerschaert et al.*, 2010] or the inverse Fourier transform approach [*Baeumer et al.*, 2005]. We approximate the operational time density $h(\tau, t)$ using a Lagrangian solver. Figures 1a and 1b show the impact of index γ on the operational time distribution. For smaller values of γ, the tail of the operational time distribution is lighter at early clock times (such as $t = 1$ in Figure 1a). For prolonged time periods, however, a smaller γ causes more dispersion of operational times (see $t = 100$ in Figure 1a). This behavior is consistent with the result in *Baeumer et al.* [2005]. When $\gamma \to 2$ and t is sufficiently large, the simulated operational time density

becomes almost symmetric (see $\alpha = 1.95$ in Figure 1b), as expected ($\gamma = 2$ is also plotted in Figure 1b for comparison); of course the subordinator as first passage time density is always positive and hence not perfectly symmetric. In addition, the capacity coefficient β acts as a scale factor that controls the width of the operational time distribution, while the mean of the distribution remains stable (Figure 1c).

4. Applications

We check the applicability of the SAE model 5 in quantifying bedload transport documented in the literature. Four bedload transport experiments were selected. Each selected study documented tracer particle snapshots (i.e., spatial distributions of sediment at specific times), and these can be used directly to explore the displacement distribution and check the feasibility of model 5. In addition, the travel distance for bed material in these cases varies from local ($\leq$ 2 m) to regional ($\sim 2,000$ m) scales, providing a wide scale range for model validation. The tracer particle size, water discharge, and the type of gravel bed (either a flume bed or natural river bed) also vary among the four cases, so that we can test the applicability of the SAE model 5 under various conditions in this section, and then analyze further the physical model in the next section.

4.1. Case 1: Small-scale mobile gravel transport in *Martin et al.* [2012]

Martin et al. [2012] traced the motion of individual gravels along a 2 meter long fixed bed built by gluing random close-packed gravel particles, where the tracer particles and the fixed bed have the same size characteristics (consisting of sorted natural gravel with the 10th, 50th, and 90th percentiles of grain diameter of 5.30 mm, 7.09 mm, and 9.13 mm, respectively). In their experiments, tracer particles moved continuously without

significant distrainments, isolating the mobile dynamics from the resting periods typical of intermittent displacement. The resultant thin-tailed, symmetric snapshot at all sampling periods (shown by symbols in Figure 2) implies a thin-tailed step length distribution.

We use model 5 to fit the first snapshot (a snapshot denotes the spatial distribution of the normalized tracer particle mass at a given sampling time), and then predict the others using the best-fit model parameters. The mean particle travel velocity, $v = 0.48$ m/s, was measured directly by *Martin et al.* [2012], so here we need not fit v. The remaining parameters (γ and β) can be fitted conveniently using the observed snapshot: while γ controls the overall shape of the snapshot, β controls the snapshot expansion (which is similar to the dispersion coefficient that controls the plume expansion). The best-fit model parameters are as follows: index $\gamma = 1.60$, and scalar $\beta = 1.0\ \mathrm{s}^{\gamma-1}$. Results show that the SAE model 5 captures the observed particle distributions (Figure 2).

4.2. Case 2: Intermediate-scale transport of sediment in *Chang and Yen* [2002]

Chang and Yen [2002] monitored the dynamics of uniform fine gravels along an 8.5 meter long flume under steady flow. Tracer particle snapshots (i.e., the distribution of normalized mass for tracer particles) were recorded for two experimental scenarios with different tracer particle sizes and flow conditions [*Chang and Yen*, 2002]. In each scenario, *Chang and Yen* [2002] fed painted tracer particles with a uniform size distribution continuously into the flume. After the feeding was done, the flow was stopped and then all the bed material was dug out for weighing. Hence the resultant snapshot (which is also the histogram of particle mass) contains particles in both motion and resting states. To obtain snapshots at various times, each scenario contains multiple experimental runs with different travel times, as shown by symbols in Figures 3 and 4. In other words, the same experiment

was repeated several times (where the flow duration was different for different runs), and therefore the measured snapshot at a later time does not depend on the previous ones.

Figure 3 shows the result from application of the SAE model 5. We fit the first snapshot (at time $t = 1$ min) using model 5, and then use the best-fit parameters to predict the late-time snapshots measured in the first experimental scenario (with a constant water discharge of 14.83 L/s, tracer size of 4.36 mm, and sediment feeding duration of 120 s). The best-fit parameters are as follows: index $\gamma = 1.60$, scalar $\beta = 8$ s$^{\gamma-1}$, and mean particle travel velocity $v = 0.017$ m/s.

We then use model 5 to capture the snapshots of the second scenario with a smaller gravel size (2.95 mm) and water discharge ($Q = 12.94$ L/s) (Figure 4). Similar to the above application, we fit the first snapshot (at time $t = 7.5$ s) and then predict the others. The best-fit parameters are as follows: $\gamma = 1.65$, $\beta = 6$ s$^{\gamma-1}$, and $v = 0.020$ m/s. It is noteworthy that the best-fit velocity v increases with the decrease of particle size, although the water discharge decreases. The fitting result for v is consistent with the size-selective transport effect, which will be discussed further in the next section.

Results show that model 5 can capture the general trend of the observed snapshots at most times. The predicted snapshots at late times can deviate from the measurements (such as Figure 3d), probably due to the fact that the late-time snapshots in *Chang and Yen* [2002] are not related to the early-time snapshots (because each experiment was run independently).

4.3. Case 3: Intermediate-scale flume experiments in *Einstein* [1937]

Einstein [1937] released more than 480 painted natural gravel clasts at a fixed cross-section in a 41 meter long straight-sided flume with relatively uniform gravel bed material.

Six tracer snapshots (which are also particle displacement distributions) were recorded for different flow strengths and flow durations (see Figure 5 symbols and Table 1). Particle displacement distributions are positively skewed for low velocities (e.g., Figure 5a) (implying the relatively strong trapping effect of particles up-flume), and they become negatively skewed at high velocities (e.g., Figure 5f) (where the trapping is relatively short).

The SAE 5 was used to fit each snapshot. Best-fit model parameters are shown in Table 1. Results show that the SAE model captures the trailing edge of the snapshot (e.g., Figure 5c,f), indicating significant retention. Here the trailing edge denotes the rear edge of the moving sediment. The thin leading edge of the SAE model snapshot also closely resembles the measurements. All of the best-fit velocities are similar to those measured in *Einstein* [1937].

4.4. Case 4: Large-scale labeled sand transport along a river bed observed by *Sayre and Hubbell* [1965]

Sayre and Hubbell [1965] monitored the transport of radioactive sand with a median grain size of 0.305 mm across a natural river bed (see symbols in Figure 6). For comparison purposes, we also apply the SAE model 5 in order to check its applicability for sediment transport along natural river beds.

Results show that the SAE model 5 captures the general trend of the evolution of sediment snapshots (see the red line in Figure 6). The best-fit mean velocity $v = 0.85$ m/hr (which is several orders of magnitude smaller than that in the above flume tests) is close to the average transport velocity for tracer sand calculated by *Sayre and Hubbell* [1965] (which is ~ 0.91 m/hr). The best-fit index is $\gamma = 1.60$, and the scalar $\beta = 3.5$ hr$^{\gamma-1}$. Note that the SAE model 5 slightly underestimates the leading edge of the measured

snapshots, due probably to the fast motion of suspended sediment [*Sayre and Hubbell*, 1965] which is beyond the modeling target of this study (see further discussion in the next section).

5. Discussion

In the following we explore the meaning and approximation for model parameters, compare the SAE model with several other bedload transport models, and discuss the limitations of the physical model. To facilitate the discussion, the above numerical analysis and model applications will be used.

5.1. Approximation of parameters in the SAE model

The three parameters used in the SAE model 5, which are v, γ, and β, have distinct physical meanings and therefore might be approximated differently.

5.1.1. Velocity v

Applications in section 4 confirm that the model velocity v in 5 represents the average particle velocity. The calculation of the average particle velocity v_r, however, may not be straightforward for practical applications. For example, many sediment particles can be buried below the active layer and therefore may not be detected easily. Fast particles may also exit the downstream boundary before the sampling cycle. In other words, it could be difficult to sample a complete distribution of particle step lengths and associated travel times. The peak position of the snapshot, however, is relatively easy to detect. Is it possible to approximate v based on the growth rate of the observed snapshot peak? To check this hypothesis, we compare the constant velocity v used in model 5 and the speed of the peak for the observed sediment snapshot (Figure 7). Results show that

v is generally close to the average growth rate of the observed snapshot peak, except for strong non-symmetric snapshots where the peak position deviates apparently from the mean displacement of sediment particles. Therefore the constant velocity v in the SAE model 5 may be approximated by the speed of the observed snapshot peak, if the observed snapshot is symmetric in a linear-linear plot. Such an approximation contains high uncertainty considering the significant discrepancy between vt and the peak of skewed snapshots, as implied by Figure 1c.

In addition, one challenge for the SAE model 5 is to determine whether the velocity v should change with time. Figures 2 and 7a suggest that the mean travel velocity for mobile sediment particles tends to remain stable with time. Figures 6 and 7c imply that the mean travel velocity of sediment particles in a regional-scale natural river does not change significantly with time. This behavior supports the constant v used in eqn. 5.

5.1.2. Index γ

The tailing index γ controls the early and late time tailing of the jump length PDF for sediment by defining the shape of the operational time distribution. For γ less than 2, the operational time distribution exhibits a negative skewness (see for example, Figure 1b), implying that a significant number of particles can move at speeds larger than the average travel velocity v (due to consecutive jumps without trapping). In addition, the trailing edge of the operational time distribution (representing slow velocities) is heavy tailed, resulting in a strong retention impact. The leading edge of the operational time distribution (representing relatively large velocities) is thin tailed, but the proportion of particles which move faster than the mean particle velocity can be larger than that for

the trailing edge, implying fast displacements (with an upper limit) of sediment particles along the bed.

The tailing index γ might be approximated using the scaling rate of the variance of sediment displacement at a late time. According to *Baeumer et al.* [2005], the variance scaling of the particle plume described by model 5 for a large time can be approximated by:

$$\sigma^2(t) \approx v^2\beta \left[\frac{4}{\Gamma(4-\gamma)} - \frac{2}{\Gamma(2-\gamma)}\right] t^{3-\gamma}\,, \tag{6}$$

although there is no analytical solution for the variance at an early time. $\Gamma(\cdot)$ in eqn. 6 denotes the Gamma function. The best-fit γ in section 4 can be validated by eqn. 6. For example, Figure 8 shows that the variance for the sediment plume from the *Sayre and Hubbell* [1965] experiment tends to scale as $\sigma^2(t) \sim t^{1.4}$, implying an index $\gamma = 1.60$ (which is the same as the best-fit γ in our model). In addition, the variance of particle displacement in *Martin et al.*'s experiment [2012] grows as $t^{1.60}$ initially, and then decreases to $t^{1.40}$ at the later time, implying an index $\gamma \approx 1.60$ (similar to the best-fit value). It is also noteworthy that eqn. 6 approximates the asymptotic scaling of variance, and therefore the variance at early times can still change with scales.

5.1.3. Capacity coefficient β

The capacity coefficient β controls the width of the operational time distribution. A larger β expands the operational time distribution, so that more tracer particles can move either faster or slower than the mean velocity v. It is noteworthy that it is not necessary for β to remain constant, although a variable β will bring additional unknown parameters. For example, for a non-stationary gravel bed (for example, a sand bar that forms in downstream zones and retards further the downstream motion of bedload sediments,

causing net deposition of particles in the system), the statistics of the operational time PDF may be space dependent, an effect that might be characterized by a space-dependent β. The transport model for sediment with mixed sizes may also require a variable β, due probably to the combination of the constant β for each uniform sediment. We will test this extension in the next section.

The capacity coefficient β is difficult to predict at present. To evaluate the trend of β varying with the water discharge and the particle size, we revisit the data-fitting applications from section 4 (Figure 9). First, when the particle size is well-sorted, the best-fit β increases nonlinearly with a decrease in the water discharge (Figure 9b) (note that the opposite trend is observed for the best-fit γ shown in Figure 9a, because a decrease in γ can also lead to a relatively heavier operational-time distribution). This trend implies that the operational time distribution may expand for a small water flux, since the probability for the long waiting times may increase for sediments when the water discharge declines. Second, when the mean velocity v remains constant, the best-fit β may decrease with an increase in the sediment size. A smaller sediment particle tends to be trapped for a longer period (due for example to the hiding effect) than a larger particle.

5.2. Comparison to other bedload transport models

Here we compare the SAE model 5 with several other bedload transport models, including the Poisson model proposed by *Einstein* [1937] and the random-walk model 1 proposed by *Bradley et al.* [2010].

First, Einstein's model and *Bradley et al.*'s model 1 [2010] are also used for case 3 (see Figure 5). Results show that the SAE solution exhibits a relatively heavier trailing edge than that for Einstein's model (see for example, Figure 5e,f), due to the heavy resting time

distribution embedded in the SAE model. The fractional-derivative model 1 proposed by *Bradley et al.* [2010] tends to slightly overestimate the leading edge of sediment fronts (due to the power-law jumps assumed by model 1), and therefore it underestimates the peak of the snapshot (see the inset in Figure 5a,d). The root-mean-square error (RMSE) for each model is also shown in Table 2: RMSE $= \sqrt{\sum(\lg P_i - \lg P_i^*)^2/n}$, where P_i and P_i^* represent the i-th modeled and measured sediment mass, respectively; and n denotes the total number of measurements. Here the logarithm of (normalized) sediment mass is used to emphasize the tailing behavior which is the critical signal of a heavy-tailed process. Although the SAE model (eqn. 5) generates a slightly higher RMSE than Einstein's model for a few experimental runs (due probably to the apparent noise in measurements), the average RMSE for all flume experiments in Case 3 is smaller for the SAE model (eqn. 5). In addition, *Bradley et al.*'s model (eqn. 1) does generate a small RMSE for some runs, such as Test No. 51 shown by Fig. 5d. However, the above analysis reveals that eqn. 1 underestimates the snapshot peak and overestimates the snapshot leading edge.

Second, the above models have been applied for case 4 by *Sayre and Hubbell* [1965] and *Bradley et al.* [2010]. Figure 6 shows the best-fit solutions for all three models. The Poisson model underestimates both tails of sediment plumes, since it assumes thin (exponential) tailed distributions for both the step length and the resting time. *Bradley et al.*'s random-walk model captures both the strong retention and the concurrent fast displacement of tracer particles. The SAE model 5 fits more closely the plume trailing tail than the other two models, but it slightly underestimates the plume leading edge. The resultant RMSE using the SAE model 5 is smaller than the other models mentioned above for most sampling cases (Table 2).

The observed power law leading edge of plumes shown in Figure 6 is most likely due to the fast motion of suspended sediment, because *Sayre and Hubbell* [1965] found that particles could temporarily be removed from the near-bed region and carried over long distances with the body of the flow. Particle step lengths for suspended sediments should differ from those for low-stage bedload transport. Typical bedload transport exhibits leading fronts relatively thinner than power law, as discussed in section 1. This is also one of the reasons that we did not add the fractional dispersion (i.e., the second term on the right-hand side of eqn. 1) into the SAE model 5.

To capture the power law plume leading edge due to suspension, we can extend slightly the SAE model 5 (see Appendix A):

$$\frac{\partial}{\partial t}P(x,t) = -v\frac{\partial}{\partial x}\frac{\partial}{\partial t}\left[-\beta(x)\frac{\partial^{\gamma}}{\partial t^{\gamma}} + \frac{\partial}{\partial t}\right]^{-1} P(x,t)\,, \tag{7}$$

where the capacity coefficient can now be space dependent. Note that when $\beta(x)$ reduces to a constant, model 7 reduces to 5. To test the applicability of a simple $\beta(x)$, we assume that β increases linearly with the travel distance. The best-fit $\beta(x) = 2.40 + 0.0045\,x$ $\mathrm{hr}^{\gamma-1}$ approaches the constant β (=3.5 $\mathrm{hr}^{\gamma-1}$) used in model 5 when the travel distance is as large as 74.4 m. The best-fit index $\gamma = 1.60$ and velocity $v = 0.85$ m/hr are the same as those fitted by model 5. Results show that the best-fit solution now captures both the plume leading and trailing edges (Figures 6c and 6d).

It is also noteworthy that the Poisson model and *Bradley et al.*'s model 1 might not be applicable for sediment dynamics observed in cases 1 and 2. On the one hand, the power-law distributed rest durations observed for case 1 [*Martin et al.*, 2012] cannot be quantified by an exponential PDF assumed by the Poisson model. The strong retention of sediment mass around the source observed in case 2 may also imply a heavy-tailed distribution for

resting times. On the other hand, the exponential distribution of particle flight lengths found in case 1 [*Martin et al.*, 2012] also challenges the fundamental assumption of power-law jump sizes in *Bradley et al.*'s model 1. None of the snapshots observed in case 2 exhibit signs of power-law jumps either.

5.3. Analysis of parameter sensitivity and the snapshot fitting sequence

In the above applications, we estimated parameters by visual fit as an initial test for our SAE model 5. The purpose of this study is to develop and then evaluate the feasibility of a new model for bedload transport dispersion. To reach this purpose, we limit all applications to visual fitting, because the previous models/applications compared by this study (including for example *Bradley et al.* [2010] and *Sayre and Hubbell* [1965]) used the same visual fitting approach. Rigorous parameter estimation and confidence intervals are therefore beyond the scope of this work. Future experimental work could more carefully and thoroughly determine the parameters for the model.

The other challenge is the snapshot fitting sequence. We used the first snapshot to fit the SAE model, and then used the best-fit parameters to predict all remaining snapshots at subsequent sampling cycles. Could a later-time snapshot be used for fitting the model? How would the fitting parameters change with the fitting sequence?

Here we conduct preliminary tests to explore the above questions. The third snapshot ($t = 2.6$ s) in case 1 [*Martin et al.*, 2012] was selected to check 1) the sensitivity of model parameters, and 2) the potential impact of snapshot fitting sequence on model parameters. Note that the last snapshot ($t = 3.6$ s) shown by Figure 2 was not selected because it contains apparent noise that may cause misleading analysis. The mean particle travel velocity ($v = 0.48$ m/s) was measured by *Martin et al.* [2012], and therefore we only

need to fit the time index γ and the capacity coefficient β in the SAE model 5. Visual fitting shows that the best fit γ (=1.6) and β (=1.0 $s^{\gamma-1}$) are the same as those fitted by the first snapshot (see section 4.1). Figure 10 also shows that, when γ is around 1.6 and $\beta = 1.0\ s^{\gamma-1}$, the SAE model 5 captures the overall trend of the snapshot better than the other values of γ and β, as also implied by the RMSE shown in Figure 11. Therefore, the snapshot fitting sequence does not significantly change the model parameters for case 1. The same conclusion is found for case 3 when the last sampling case (i.e., $t = 216.5$ hrs shown in Figure 6d) is used (not shown here).

Figure 10 also shows that, on the one hand, expansion of the sediment snapshot is sensitive to the capacity coefficient β, a parameter that controls the expansion of the operational time distribution. On the other hand, the scale index γ affects the skewness of the snapshot, because it affects both the early and late time tailings of sediment transport. Similar conclusions can also be found for case 3 (not shown here).

5.4. Limitations of the SAE model 5

There are two major limitations of the SAE model. First, the SAE model 5 limits to steady flow. Whether it can capture non-steady flow, such as the bed armoring process with a mixed bed, remains to be shown. The second major limitation is that the SAE model 5 can only describe a super-diffusive displacement at a large time, as indicated by eqn. 6. As discussed above, the combination of slow and fast moving particles enhances the growth rate of the variance for particle displacements, which can be faster than that for Fickian diffusion. However, *Nikora et al.* [2002] suggested that bedload transport at a global range is likely to be subdiffusive ("sub-diffusion" means that the variance of particle displacement grows slower than linear in time, a process that can be captured

using the index $0 < \gamma < 1$ in eqn. 2 [*Zhang et al.*, 2012]), due to the increased probability of long periods of trapping when the travel time is large. If the PDF of the waiting time distribution changes with scale (in either space or time), then model parameters in 5 are no longer expected to be constant. In this case, the constant-parameter model 5 may be extended to a SAE model with a variable capacity coefficient $\beta(x,t)$ (see model 7), a variable index $\gamma(x,t)$ (where γ can be in the range of $[0,1]$), and/or a variable velocity (due to transient flows, for example). For instance, when $0 < \gamma < 1$, the variance of sediment tracer displacements grows as $\sigma^2(t) \approx v^2[2/\Gamma(1+2\gamma) - 1/(\Gamma(1+\gamma)^2)]t^{2\gamma}$ [*Baeumer et al.*, 2005], which describes subdiffusion for $\gamma < 0.5$. Further examples and the hydrological background of the variable-index fractional-derivative models can be found in *Sun et al.* [2014a]. We will explore further the above two limitations in a future study.

5.5. Extension of the SAE model for mixed-size sediment transport

We also conduct flume experiments to check whether the SAE model 5 or its extension 7 can capture transport dynamics of a mixed-size sediment. Further comparison can also be made for the above fractional-derivative models using additional, first-hand data. Our flume experiments are similar to those in *Chang and Yen* [2002], except that we use the mixed sand for both the tracer sediment and the bed. Detailed description of the experiments can be found in *Sun et al.* [2014b].

Figure 12 shows that the SAE model 5 with a constant β can efficiently fit the snapshot for each size tracer particle transport along a mixed bed. Comparison shows that the SAE model 5 describes the trailing edge and the peak of the measured snapshot slightly better than the general fADE model 2, although the measurements contain apparent noises.

Figure 13 further shows that the extended SAE model 7 captures the leading tail and the skewness of the observed snapshot for the mixed-size sediment slightly better than the SAE model 5. Here we use only very coarse sand as tracer particles. The leading edge of sediment front might be more apparent with an increase in the gravel size distribution (such as mixing with finer sand). This result is consistent with the conclusion in *Hill et al.* [2010], who found a heavier distribution of travel distance for a wider grain size distribution. Mixing over different particle sizes may alter the distribution of step lengths and/or resting times along tracer particle trajectories, resulting in a space-dependent operational time distribution. In addition, individual tracer particles transport along a mixed bed may not be independent, due to interactions between particles with various sizes. The SAE model and its extension however treat each tracer particle as an independent random walker. Successful applications of the SAE model imply that the dependent sediment dynamics might be simplified as an independent CTRW process. We will systematically conduct flume experiments to evaluate the above hypotheses.

6. Conclusions

This study is aimed at simplifying previous fractional-derivative models in order to quantify uniform bedload sediment transport across a wide range of scales. Comparisons and applications of the nonlocal transport models may also enhance our understanding of the complex random nature in sediment transport. Numerical analysis and model applications reveal four major conclusions.

First, the SAE model 5 simplifies the spatiotemporal fADE model 2 by removing the unpredictable dispersion coefficient and the spatial nonlocal term. The subordination scheme used in the SAE model captures the random time for bedload sediment particles

spent between two subsequent jumps. Applications show that the SAE model efficiently characterizes the observed transport for uniform bedload sediment at all scales. Successful applications of the SAE model also imply that 1) the mean waiting time for bedload sediment can be finite (while the variance is infinite due to the wide distribution of the trapping period), and 2) a universal type of PDF (describing the heavy-tailed waiting time distribution and the relatively lighter tailed step length distribution that are well documented in the literature) does exist for a typical, uniform bedload transport process.

Second, all of the three parameters in the SAE model 5 have specific meanings. For example, the velocity v represents the average particle velocity of travel. The time index γ affects the early and late time tailing behavior of sediment transport by controlling the skewness of the operational time distribution. The capacity coefficient β scales the operational time distribution. Applications further show that γ and β may depend on particle size and water discharge. The model parameters therefore may vary with a single physical process. It is noteworthy that the SAE model 5 with constant parameters controls the average dynamics of sediment transport reaching ergodicity. How to increase the model predictability therefore requires further study, as is the case for other fractional-derivative models used in other hydrological and geophysical processes [*Zhang et al.*, 2014].

Third, events at the extreme edge of the probability distribution for trapping and jumping processes provide signals for anomalous dynamics of bedload sediment transport and therefore should be the emphasis of future laboratory/field observations. The combination of parameters γ and β defines the operational time distribution and captures the sediment dynamics, and therefore observations of uniform bedload sediment transport may be focused on specific transport properties. For example, measurements of long waiting

times (especially for sediments trapped near the initial source) are important because they can be used to evaluate whether the long waiting times (corresponding to the small operational times) are heavy tailed. Measurements of large down-flume displacement of sediments may also be needed, since they provide useful information for the tailing behavior of step length distribution which correspond to the large operational times.

Fourth, the SAE model may be extended to account for additional dynamics. For example, to capture the regional-scale transport mixed with suspension, the capacity coefficient β in the SAE model may change with the travel distance. For a stationary system, however, constant parameters in the SAE model can be used to capture time-dependent scaling rates of moments for particle displacements. In addition, our preliminary flume experiments show that the SAE model can be extended to quantify the mixed-size bedload transport, implying that the dependent sediment dynamics might be simplified as an independent CTRW process. Further validations are needed for the above extensions.

Appendix A: Derivation of the SAE model with a space-dependent capacity coefficient $\boldsymbol{\beta(x)}$

Baeumer et al. [2005] showed that the first passage time density (which is also the operational time density $h(\tau, t)$) of a Lévy stable process with drift solves

$$\left(-\beta D_t^\gamma + \frac{\partial}{\partial t}\right) h(\tau, t) = -\frac{\partial}{\partial \tau} h(\tau, t) + f(\tau)\delta(t), \tag{A1}$$

with $h(\tau, 0) = \delta(\tau); h(0, t) = h_t(\tau, 0) = 0$ and the requirement that the solution is a integrable, which uniquely determines f. Furthermore the fractional derivative D_t^γ is a Caputo derivative; i.e.,

$$D_t^\gamma h = \int_0^t \frac{(t-s)^{1-\gamma}}{\Gamma(2-\gamma)} \frac{d^2}{ds^2} h(s)\, ds.$$

Taking Laplace transforms it is straightforward to see that eqn. A1 is equivalent to

$$\left(-\beta\frac{\partial^\gamma}{\partial t^\gamma}+\frac{\partial}{\partial t}\right)h(\tau,t)=-\frac{\partial}{\partial\tau}h(\tau,t), \tag{A2}$$

with $h(\tau,0)=\delta(\tau); h(0,t)=0$, where we define the fractional derivative $\frac{\partial^\gamma}{\partial t^\gamma}$ as a first degree Caputo derivative; i.e.,

$$\frac{\partial^\gamma}{\partial t^\gamma}h=\frac{d}{dt}\int_0^t\frac{(t-s)^{1-\gamma}}{\Gamma(2-\gamma)}\frac{d}{ds}h(s)\,ds=\frac{d}{dt}D_t^{\gamma-1}h.$$

In this representation the uniquely determined function f enters as an initial value function; i.e. $f=D_t^{\gamma-1}h(0)$ and does not need to be specified in the equation.

This subordinator equation can now be embedded into the classical advection-dispersion framework replacing $-\frac{\partial}{\partial\tau}$ with the linear spatial operator derived from the continuity equation

$$\frac{\partial C}{\partial t}+\nabla\cdot F=0. \tag{A3}$$

That is, if $\nabla\cdot F=-AC$ for some linear operator A, the function

$$P(x,t)=\int_0^\infty h(t,\tau)C(x,\tau)\,d\tau, \tag{A4}$$

obtained by randomizing the time variable of the classical solution $C(x,t)$ of eqn. A3 according to the subordinator h satisfies

$$\left(-\beta\frac{\partial^\gamma}{\partial t^\gamma}+\frac{\partial}{\partial t}\right)P(x,t)=AP(x,t);\quad P(x,0)=P_0(x).$$

For example in case of the advection-dispersion equation $A=-\nabla\cdot(v-D\nabla)$ we obtain model 4

$$\left(-\beta\frac{\partial^\gamma}{\partial t^\gamma}+\frac{\partial}{\partial t}\right)P(x,t)=AP(x,t);\quad P(x,0)=P_0(x). \tag{A5}$$

In order to make the waiting time process spatially dependent we need to be careful to still observe the continuity equation. For that we need to rewrite A5 and partially

differ-integrate both sides; i.e., if L_t is the derivative operator $L_t = \left(-\beta \frac{\partial^\gamma}{\partial t^\gamma} + \frac{\partial}{\partial t}\right)$ we need to apply $\frac{\partial}{\partial t} L_t^{-1}$ (defined by the reciprocal of the Laplace transform symbol of L_t) to both sides of eqn. A2 and obtain

$$\frac{\partial}{\partial t} P(x,t) = A \frac{\partial}{\partial t} L_t^{-1} P(x,t). \tag{A6}$$

This identifies the concentration of particles available to take part in the spatial process (the mobile particles) as $\frac{\partial}{\partial t} L_t^{-1} P(x,t)$. In this formulation it is now justified to make L_t^{-1} spatially dependent (via $\beta(x)$, for example, as used in eqn. 7) and obtain the governing equation of the process approximated by the spatially dependent Lagrangian solver.

Acknowledgments. This work was supported by the State Key Laboratory of Hydrology-Water Resources and Hydraulic Engineering under grant 2013490111, the National Natural Science Foundation of China under 11202066, the National Science Foundation of the U.S. under grant DMS-1025417 and DMS-1460319, and the State Water Research Institute Program of the U.S. Geological Survey under 2013NV196B. Any opinions, findings, conclusions, or recommendations do not necessarily reflect the views of the funding agencies. We thank the Editor (Alexander Densmore), the Associate Editor (Bruce MacVicar), and three reviewers (Vaughan Voller and two anonymous reviewers) for insightful suggestions that significantly improved this work.

References

Baeumer, B., M. M. Meerschaert, D. A. Benson, and S. W. Wheatcraft (2001), Subordinated advection-dispersion equation for contaminant transport, *Water Resour. Res.*, *37*(6), 1543-1550.

Baeumer, B., D. A. Benson, and M. M. Meerschaert (2005), Advection and dispersion in time and space, *Phys. A, 350*(2-4), 245–262.

Baeumer, B., and M. M. Meerschaert (2007), Fractional diffusion with two time scales, *Phys. A, 373*, 237–251.

Bennett, S. J., and J. S. Bridge (1995), An experimental-study of flow, bedload transport and bed topography under conditions of erosion and deposition and comparison with theoretical-models, *Sedimentology, 42*(1), 117–146.

Bombar, G., S. Elci, G. Tayfur, S. Guney, and A. Bor (2011), Experimental and numerical investigation of bed-load transport under unsteady flows, *J. Hydraul. Eng., 137*(10), 1276–1282.

Bradley, D. N., G. E. Tucker, and D. A. Benson (2010), Fractional dispersion in a sand bed river, *J. Geophys. Res., 115*, F00A09, doi:10.1029/2009JF001268.

Chang, S. Y., and C. L. Yen (2002), Simulation of bed-load dispersion process, *J. Hydraul. Eng., 128*(3), 331–342.

Cudden, J., and T. Hoey (2007), The causes of bedload pulses in a gravel channel: The implications of bedload grain-size distributions, *Earth Surf. Proc. Land., 28*(13), 1411–1428, doi:10.1002/esp.521.

Dancey, C. L., P. Diplas, A. Papanicolaou, and M. Bala (2002), Probability of individual grain movement and threshold condition, *J. Hydraul. Eng., 128*, 1069–1075.

Eaton, B. C., and M. Church (2009), Channel stability in bed-dominated streams with nonerodible banks: Inferences from experiments in a sinuous flume, *J. Geophys. Res., 114*, F01024, doi:10.1029/2007JF000902.

Einstein, H. A. (1937), Bed load transport as a probability problem (in German), Ph.D. thesis, ETH Zurich. (English translation by W. W. Sayre, In *Sedimentation*, Appendix C, edited by H.-W. Shen, pp. C1-C105, Colo. State Univ., Fort Collins, Colo., 1972.)

Ferguson, R., T. Hoey, S. Wathen, and A. Werritty (1996), Field evidence for rapid downstream fining of river gravels through selective transport, *Geology, 24*(2), 179–182.

Fraccarollo, L., and G. Rosatti (2009), Lateral bed load experiments in a flume with strong initial transversal slope, in sub- and supercritical conditions, *Water Resour. Res., 45*, W01419, doi:10.1029/2008WR007246.

Ganti, V., M. M. Meerschaert, E. Foufoula-Georgiou, E. Viparelli, and G. Parker (2010), Normal and anomalous dispersion of gravel tracer particles in rivers, *J. Geophys. Res., 115*, F00A12, doi:10.1029/2008JF001222.

Harman, C., D. M. Reeves, B. Baeumer, and M. Sivapalan (2010), A subordinated kinematic wave equation for heavy-tailed flow responses from heterogeneous hillslopes, *J. Geophys. Res., 115*, F00A08, doi:10.1029/2009JF001273.

Haschenburger, J. K., and P. R. Wilcock (2003), Partial transport in a natural gravel bed channel, *Water Resour. Res., 39*(1), 1020, doi:10.1029/2002WR001532.

Hill, K. M., L. Dellangelo, and M. M. Meerschaert (2010), Heavy-tailed travel distance in gravel bed transport: An exploratory enquiry, *J. Geophys. Res., 115*, F00A14, doi:10.1029/2009JF001276.

Hodge, R. A., T. B. Hoey, and L. S. Sklar (2011), Bed load transport in bedrock rivers: The role of sediment cover in grain entrainment, translation, and deposition, *J. Geophys. Res., 116*, F04028, doi:10.1029/2011JF002032.

Houssais, M., and E. Lajeunesse (2012), Bedload transport of a bimodal sediment bed, *J. Geophys. Res., 117*, F04015, doi:10.1029/2012JF002490.

Johnson, J. P., and K. X. Whipple (2007), Feedbacks between erosion and sediment transport in experimental bedrock channels, *Earth Surf. Proc. Land., 32*(7), 1048–1062.

Kumar, A., M. M. Meerschaert, and P. Vellaisamy (2011), Fractional normal inverse Gaussian diffusion, *Stat. Probabil. Lett., 81*, 146–152.

Lajeunesse, E., L. Malverti, and F. Charru (2010), Bed load transport in turbulent flow at the grain scale: Experiments and modeling, *J. Geophys. Res., 115*, doi:10.1029/2009JF001628.

Lee, K. T., Y. L. Liu, and K. H. Cheng (2004), Experimental investigation of bedload transport processes under unsteady flow conditions, *Hydrol. Process., 18*(13), 2439-2454.

Lenzi, M. A., L. Mao, and F. Comiti (2006), Effective discharge for sediment transport in a mountain river: Computational approaches and geomorphic effectiveness, *J. Hydrol., 326*, 257–276.

Madej, M. A., D. G. Sutherland, T. E. Lisle, and B. Pryor (2009), Channel responses to varying sediment input: A flume experiment modeled after Redwood Creek, California, *Geomorphology, 103*(4), 507–519.

Marion, A., M. Zaramella, and A. Bottacin-Busolin (2008), Solute transport in rivers with multiple storage zones: The STIR model, *Water Resour. Res., 44*, W10406, doi:10.1029/2008WR007037.

Martin, R. L., D. J. Jerolmack, and R. Schumer (2012), The physical basis for anomalous diffusion in bed load transport, *J. Geophys. Res., 117*, doi:10.1029/2011JF002075.

Meerschaert, M. M., Y. Zhang, and B. Baeumer (2010), Particle tracking for fractional diffusion with two time scales, *Comput. Math. Appl., 59*, 1078-1086.

Meerschaert, M. M., and A. Sikorskii (2012), *Stochastic Models for Fractional Calculus*, De Gruyter Studies in Mathematics, Vol. 43, ISBN 978-3-11-025869-1.

Metzler, R., and J. Klafter (2000), The random walks guide to anomalous diffusion: A fractional dynamic approach, *Phys. Rep., 339*, 1-77.

Miller, K. S., and B. Ross (1993), *An Introduction to Fractional Calculus and Fractional Differential Equations*, John Wiley, Hoboken, N. J.

Nikora, V., H. Habersack, T. Huber, and I. McEwan (2002), On bed particle diffusion in gravel bed flows under weak bed load transport, *Water Resour. Res., 38*(6), 1081, doi:10.1029/2001WR000513.

Niño, Y., F. Lopez, and M. Garcia (2003), Threshold for particle entrainment into suspension, *Sedimentology, 50*, 247–263.

Park, G., and P. C. Klingeman (1982), On why gravel bed streams are paved, *Water Resour. Res., 18*(5), 1409–1423.

Pecking, A. (2009), Theoretical development on the effects of changing flow hydraulics on incipient bed load motion, *Water Resour. Res., 45*, W04401, doi:10.1029/2008WR006826.

Pyrce, R. S., and P. E. Ashmore (2003a), The relation between particle path length distributions and channel morphology in gravel-bed streams: a synthesis, *Geomorphology, 56*, 167–187.

Pyrce, R. S., and P. E. Ashmore (2003b), Particle path length distributions in meandering gravel-bed streams: Results from physical models, *Earth Surf. Proc. Land., 28*(9), 951–

966.

Sayre, W., and D. Hubbell (1965), *Transport and dispersion of labeled bed material, North Loup River, Nebraska*. U. S. Geol. Surv. Prof. Pap. 433-C, 48 pp.

Schmidt, K., and P. Ergenzinger (1992), Bedload entrainment, travel lengths, step lengths, rest periods - Studied with passive (iron, Magnetic) and active (radio) tracer techniques, *Earth Surf. Proc. Land., 17*(2), 147–165, doi:10.1002/esp.3290170204.

Schumer, R., M. M. Meerschaert, and B. Baeumer (2009), Fractional advection-dispersion equations for modeling transport at the Earth surface, *J. Geophys. Res., 114*, F00A07, doi:10.1029/2008JF001246.

Sear, D., A. (2006), River restoration and geomorphology, *Aquat. Conserv., 4*(2), 169–177, doi:10.1002/aqc.v4:2/issuetoc.

Shields Jr., F. D., R. R. Copeland, P. C. Klingeman, M. W. Doyle, and A. Simon (2003), Design for stream restoration, *J. Hydraul. Eng.-ASCE, 129*(8), 575–584.

Stark, C., E. Foufoula-Georgiou, and V. Ganti (2009), A nonlocal theory of sediment buffering and bedrock channel evolution, *J. Geophys. Res., 114*, F01029, doi:10.1029/2008JF000981.

Strom, K., A. N. Papanicolaou, N. Evangelopoulos, and M. Odeh (2004), Microforms in gravel bed rivers: Formation, disintegration, and effects on bedload transport, *J. Hydraul. Eng., 130*(6), 554–567.

Sun, H. G., Y. Zhang, W. Chen, and D. M. Reeves (2014a), Use of a variable-index fractional-derivative model to capture transient dispersion in heterogeneous media, *J. Contam. Hydrol., 157*, 47–58.

Sun, H. G., D. Chen, Y. Zhang, and L. Chen (2014b), An improved understanding of anomalous transport of sediment along a mixed bed using flume experiments and stochastic model analysis, *J. Hydrol.*, in preparation.

Tritthart, M., B. Schober, and H. Habersack (2011), Non-uniformity and layering in sediment transport modeling 1: flume simulations, *J. Hydraul. Res., 49*(3), 325–334.

Wilcock, P. R. (1992), *Experimental investigation of the effect of mixture properties on transport dynamics*. In: Billi, P. et al. (Ed.), Dynamics of Gravel-bed Rivers, John Wiley, New York, pp. 109–139.

Wong, M., G. Parker, P. DeVries, T. M. Brown, and S. J. Burges (2007), Experiments on dispersion of tracer stones under lower-regime plane-bed equilibrium bed load transport, *Water Resour. Res., 43*, W03440, doi:10.1029/2006WR005172.

Zhang, Y., M. M. Meerschaert, and A. I. Packman (2012), Linking fluvial bed sediment transport across scales, *Geophys. Res. Lett., 39*, L20404, doi:10.1029/2012GL053476.

Zhang, Y., C. Green, and B. Baeumer (2014), Linking aquifer spatial properties and non-Fickian transport in mobile-immobile like alluvial settings, *J. Hydrol., 512*, 315–331.

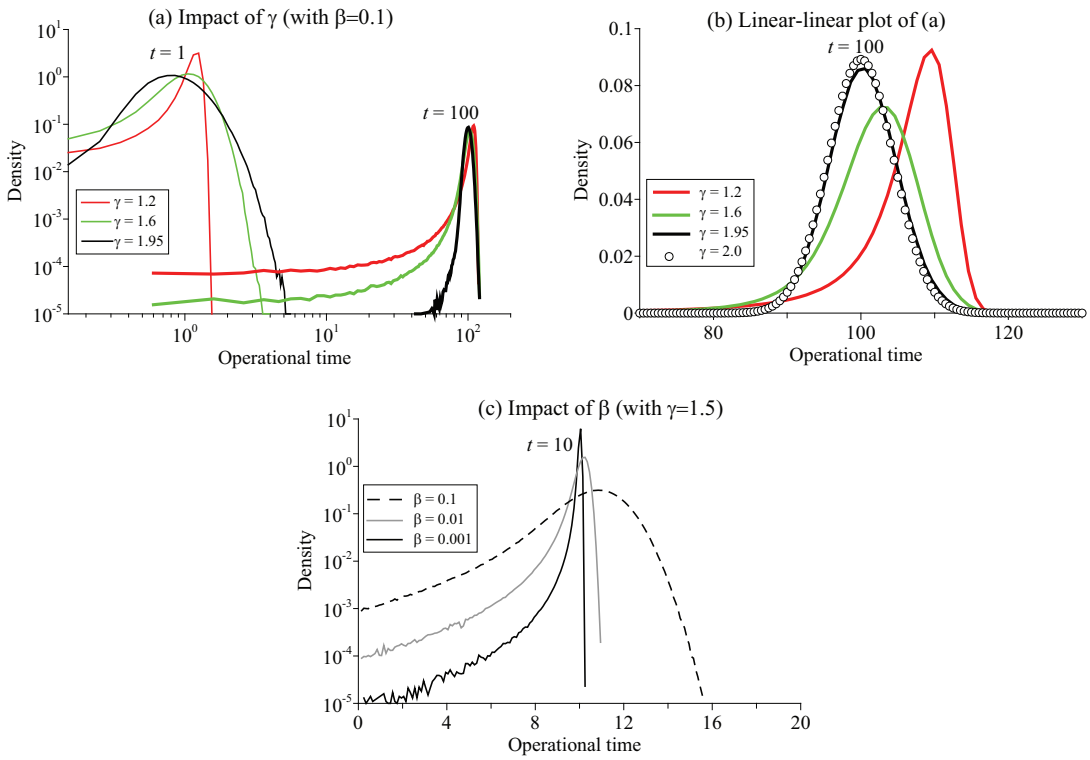

Figure 1. Examples of the operational time (τ) simulation using the Lagrangian solver. (a) The density of operational time corresponding to clock time $t = 1$ and $t = 100$, respectively. Various indexes γ are tested. The operational time smaller or larger than the clock time represents sediment particles moving slower or faster than the mean velocity. (b) shows the linear-linear plot of (a), emphasizing the density at clock time $t = 100$. (c) shows the impact of capacity coefficient β on the density of operational time.

Figure 2. Case 1: Modeled (lines, using the SAE model 5) versus observed (symbols) snapshots for uniform tracer particles measured by *Martin et al.* [2012]. (b) is the semi-log plot of (a), to show the tailing and the particle number density in the immobile phase.

Figure 3. **Case 2**: Modeled (lines, using the SAE model 5) versus observed (symbols) snapshots for uniform tracer particles with a diameter of **4.36** mm measured by *Chang and Yen* [2002] at times $t = 1$ min (a), 3 min (b), 5 min (c), and 7 min (d), respectively.

Figure 4. **Case 2**: Modeled (lines, using the SAE model 5) versus observed (symbols) snapshots for uniform tracer particles with a diameter of **2.95** mm measured by *Chang and Yen* [2002] at times $t = 7.5$ s (a), 22.5 s (b), 37.5 s (c), 52.5 s (d), 67.5 s (e), and 82.5 s (f), respectively.

Figure 5. Case 3: *Einstein*'s (1937) experiments: The normalized mass fitted by the SAE model 5 (the red line) versus the measurements (symbols). The best-fit parameters using 5 are listed in Table 1. For comparison purposes, the solution of Einstein's Poisson model (the blue dashed line) and *Bradley et al.*'s model 1 [2010] (the black dotted line) are also shown. The inset in (a) and (d) is the linear-linear plot, to show the peak.

Table 1. Einstein's flume experiments: Model parameters used to capture the sediment snapshots (which are also the path length distributions) from *Einstein*'s [1937] flume experiments. In the legend, 'T' denotes the flow duration, 'R' is the gravel size (which is the smallest diameter; see *Einstein* [1937]), γ is the time index, β is the capacity coefficient, v is the best-fit velocity, and v_r is the average particle velocity measured by *Einstein* [1937].

Run	T (min)	Gravel size (mm)	γ	β ($s^{\gamma-1}$)	v (m/s)	v_r (m/s)
Fig. 5a	5	$R < 17$	1.43	7.0	1.24×10^{-2}	1.24×10^{-2}
Fig. 5b	60	$17 < R < 24$	1.35	8.0	1.67×10^{-3}	1.58×10^{-3}
Fig. 5c	5	$17 < R < 24$	1.45	4.0	2.97×10^{-2}	2.97×10^{-2}
Fig. 5d	20	$17 < R < 24$	1.43	5.2	6.84×10^{-3}	6.84×10^{-3}
Fig. 5e	6	$R < 17$	1.55	3.5	3.32×10^{-2}	3.55×10^{-2}
Fig. 5f	3	$R > 24$	1.53	1.3	1.04×10^{-1}	1.10×10^{-1}

Figure 6. Case 4: Concentration profiles at various times modeled by the SAE model (solid red line) versus measurements of *Sayre and Hubbell* [1965] (symbols). The model results of *Bradley et al.* [2010] (dotted black lines; using model 1) and *Sayre and Hubbell* [1965] (dashed blue line; using Einstein's Poisson model) are also shown for comparison. The right column shows the linear-linear plot of the left column. The solid green line shows the best-fit solution using model 7.

Figure 7. Velocity of the peak for the observed sediment snapshot versus the best-fit mean particle velocity: (a) Case 1 [*Martin et al.*, 2012]; (b) Case 3 [*Einstein*, 1937]; and (c) Case 4 [*Sayre and Hubbell*, 1965]. In (a), at the last sampling cycle, there are multiple peaks in the observed snapshot, and velocities are shown for both the observed 1st and 2nd peaks.

Figure 8. The variance scaling of the data (symbols) and the power-law trendline ($\sim t^{1.4}$) for sediment displacement from the Sayre and Hubbell experiment [*Sayre and Hubbell*, 1965]. Note that the last several measurements are not included in analyzing the trendline, since the observations at late times are incomplete [*Bradley et al.*, 2010] and therefore contain high uncertainty.

Figure 9. Relationship between the best-fit average particle velocity and parameter γ (a), and parameter β (b). The size of the symbol represents the relative size of the tracer sediment. The maximum and minimum diameters of the tracer sediment are $R > 24$ mm and $R = 0.305$ mm, respectively.

Table 2. The root-mean-square error showing the differences between model predictions and measurements for *Einstein*'s flume experiments **(Case 3)** and *Sayre and Hubbell*'s tracer test **(Case 4)**. In the legend, "Sample N" denotes the number of measurements; "SAE 5" means the subordinated advection equation 5; "fADE 1" represents the fractional advection-dispersion equation 1; and "SAE 7" is the subordinated advection equation 7 with a space-dependent capacity coefficient.

Run	Sample N	SAE 5	Einstein's model	fADE 1	SAE 7
Case 3 - Fig. 5a	18	0.13	0.16	0.19	–
Case 3 - Fig. 5b	19	0.46	0.44	0.37	–
Case 3 - Fig. 5c	20	0.25	0.28	0.35	–
Case 3 - Fig. 5d	18	0.43	0.45	0.39	–
Case 3 - Fig. 5e	16	0.26	0.18	0.16	–
Case 3 - Fig. 5f	18	0.16	0.25	0.21	–
Case 4 - Fig. 6a	40	0.28	0.44	0.37	0.30
Case 4 - Fig. 6b	40	0.31	0.55	0.32	0.26
Case 4 - Fig. 6c	49	0.25	0.93	0.25	0.20
Case 4 - Fig. 6d	39	0.17	1.26	0.15	0.10
Case 4 - Average	42	0.26	0.86	0.29	0.23

Figure 10. Sensitivity analysis for the time index γ (a) and the capacity coefficient β (c) used in the SAE model 5 for case 1 at the sampling time $t = 2.6$ s. (b) and (d) are the log-log plot of (a) and (b), respectively, to show the tailing. In (a), $\beta = 1.0$ s$^{\gamma-1}$. In (c), the unit of β is s$^{\gamma-1}$, and $\alpha = 1.6$.

Figure 11. Relationship between the RMSE and the time index γ in the SAE model 5 for case 1 at the sampling cycle $t = 2.6$ s.

Figure 12. The measured sediment snapshots (circles) versus the model simulations (lines) for each size tracer particle. The black line is the best-fit solution using the spatiotemporal fADE model 2, and the red line is the model fit using the SAE model 5. In the legend, 'R' denotes the gravel size, 'T_1' is the flow duration, and 'T_2' is the feeding time of tracer particles at the inlet.

Figure 13. The measured sediment snapshots (circles) versus the model simulations (lines) for the mixed-size sediment. The black line is the best-fit solution using the SAE model 5 with a constant parameter $\beta = 2.4$ min$^{\gamma-1}$ (and $\gamma = 1.45$), while the grey line is the solution using the extended SAE model 7 with a variable β. In this experimental run, the flow duration is 27.03 min, and the feeding time of tracer particles is 10 min.

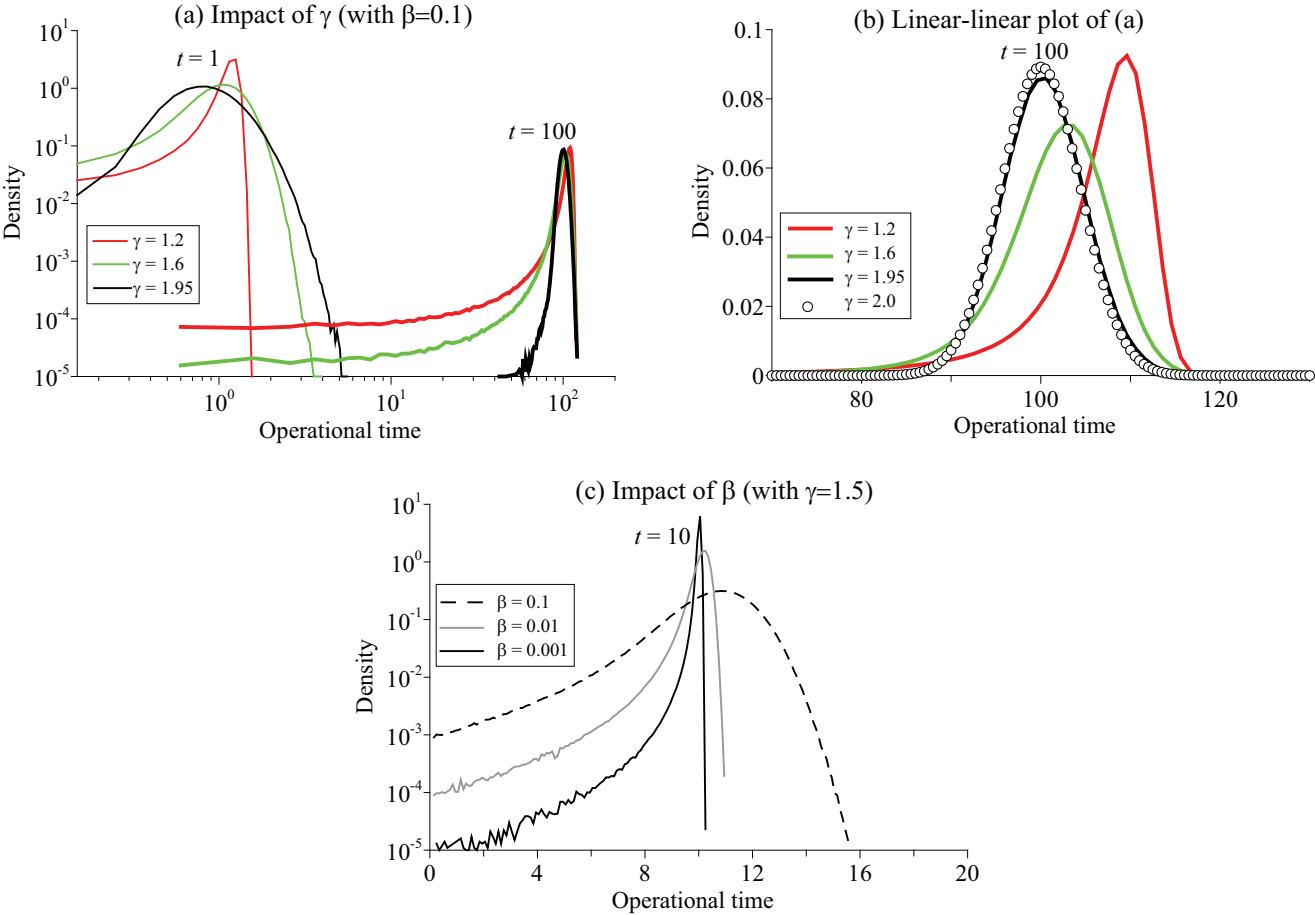
(a) Impact of γ (with β=0.1)
t = 1
t = 100
Density
γ = 1.2
γ = 1.6
γ = 1.95
Operational time
(b) Linear-linear plot of (a)
t = 100
Density
γ = 1.2
γ = 1.6
γ = 1.95
γ = 2.0
Operational time
(c) Impact of β (with γ=1.5)
t = 10
Density
β = 0.1
β = 0.01
β = 0.001
Operational time

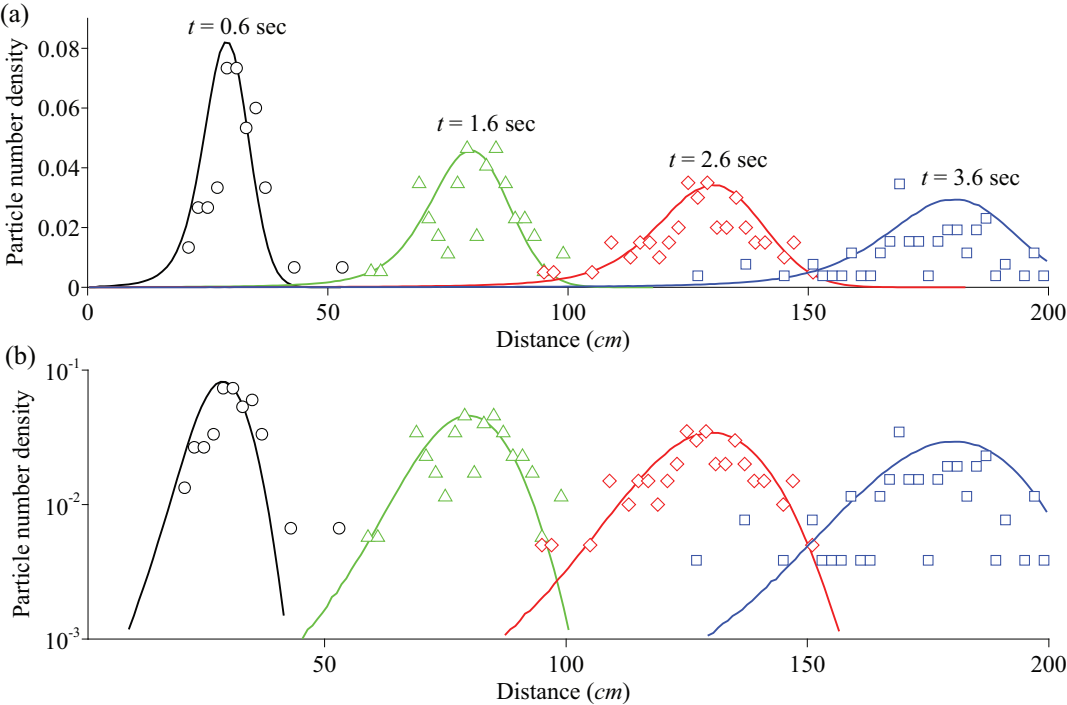
(a)
t = 0.6 sec
t = 1.6 sec
t = 2.6 sec
t = 3.6 sec
Particle number density
0.08
0.06
0.04
0.02
0
0
50
100
150
200
Distance (cm)
(b)
Particle number density
10-1
10-2
10-3
50
100
150
200
Distance (cm)

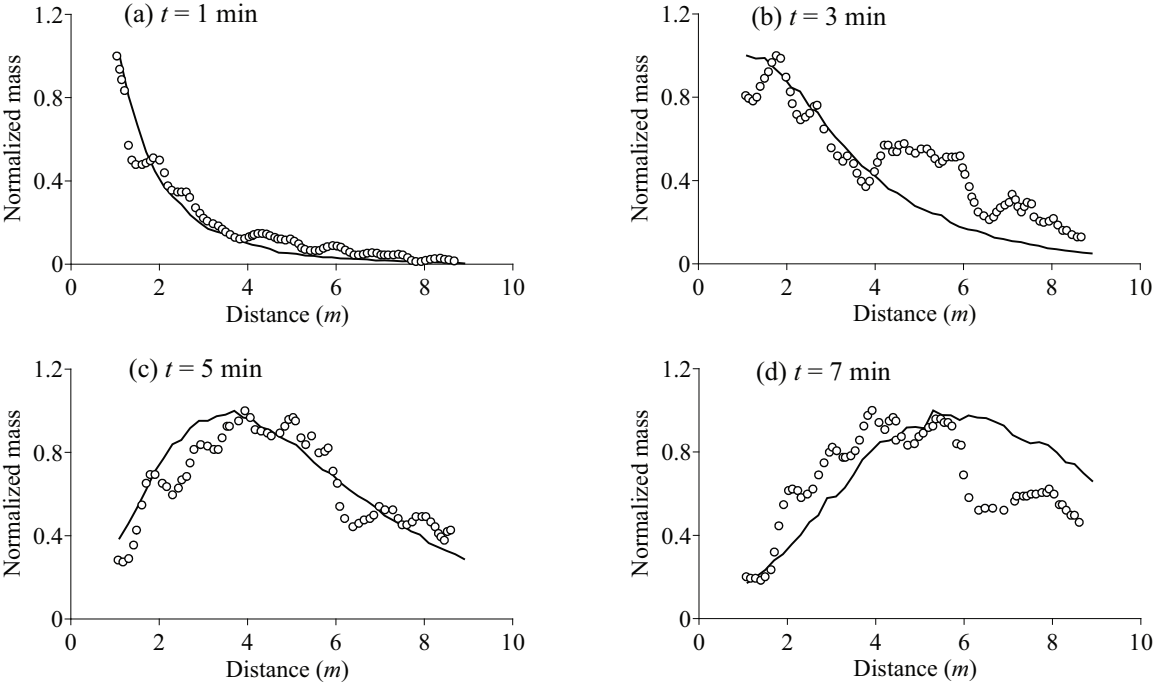
(a) t = 1 min
(b) t = 3 min
(c) t = 5 min
(d) t = 7 min
Normalized mass
Distance (m)
0
0.4
0.8
1.2
2
4
6
8
10

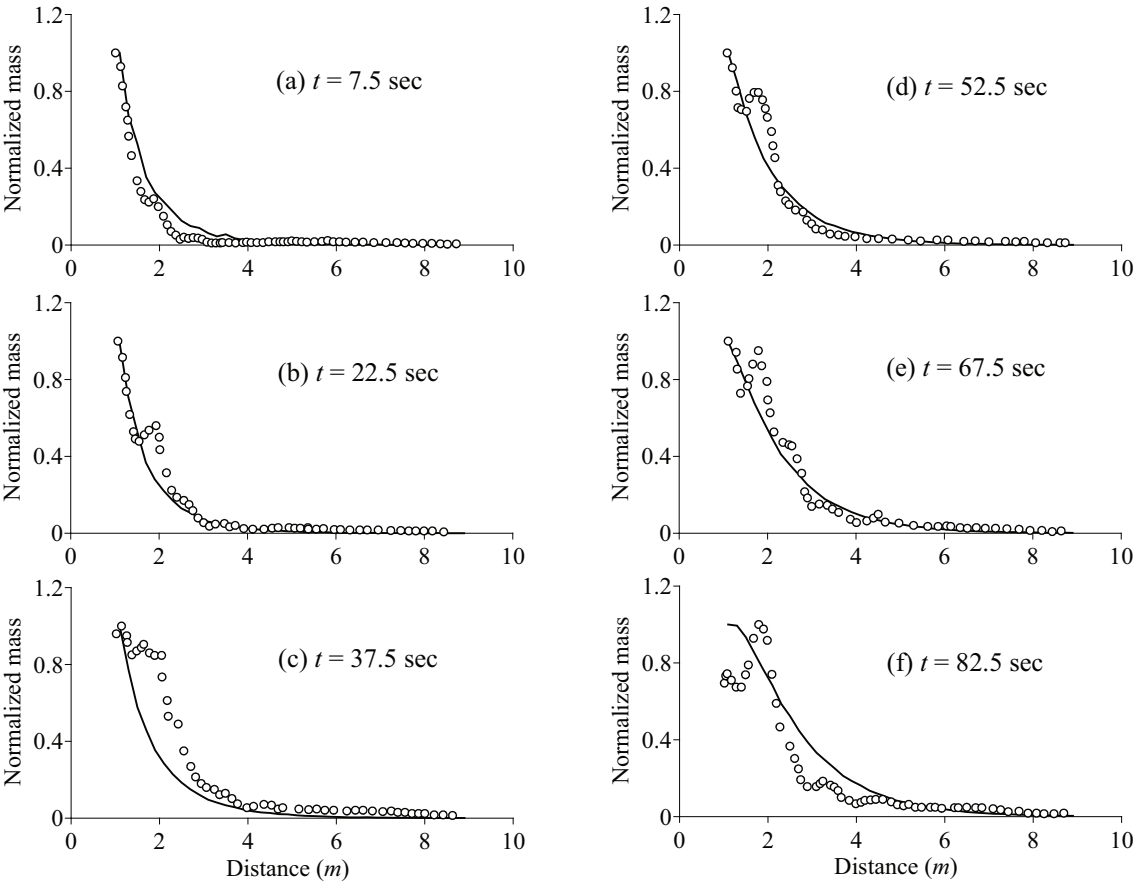
(a) t = 7.5 sec
(b) t = 22.5 sec
(c) t = 37.5 sec
(d) t = 52.5 sec
(e) t = 67.5 sec
(f) t = 82.5 sec
Normalized mass
Distance (m)
0
0.4
0.8
1.2
2
4
6
8
10

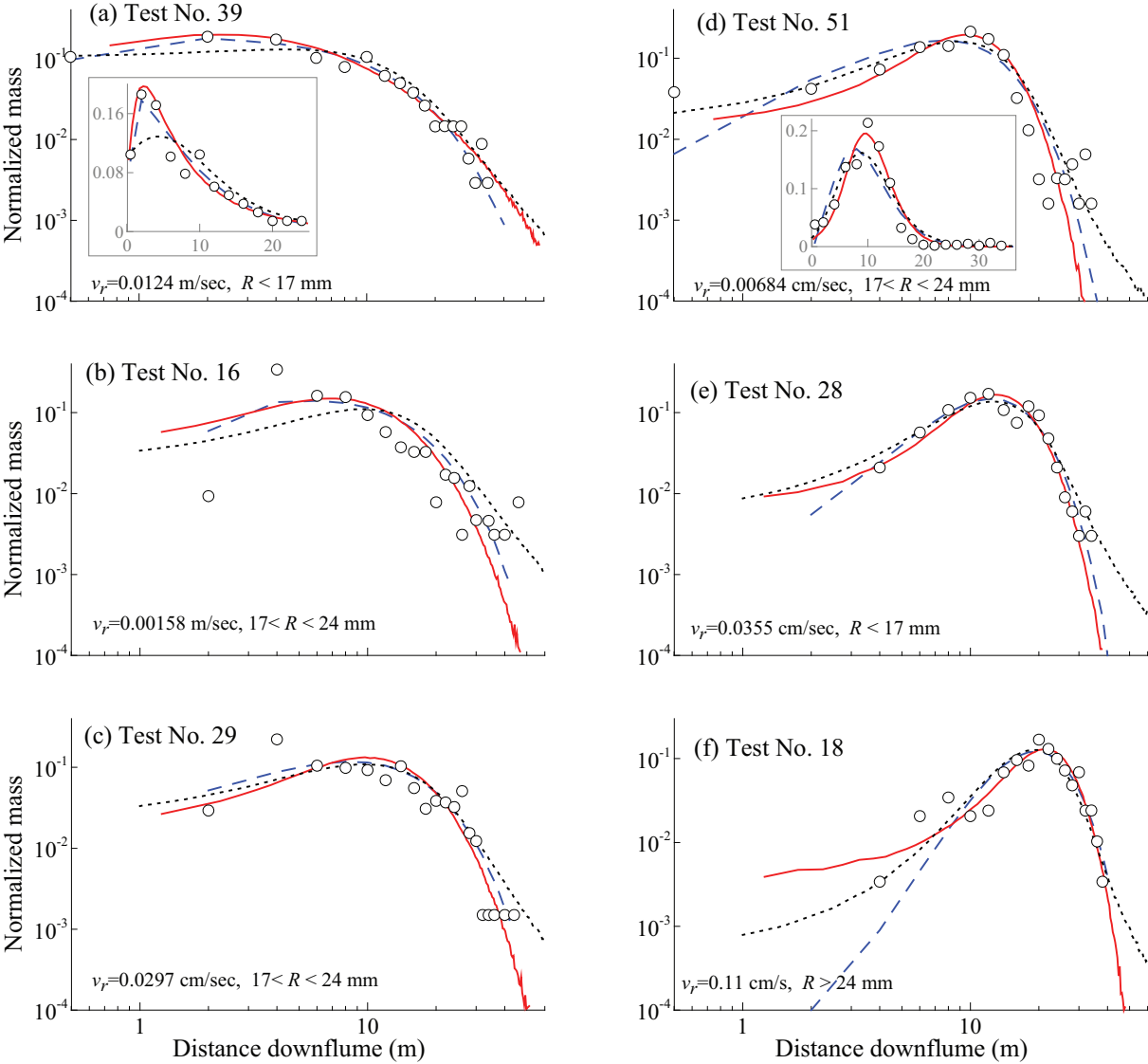
(a) Test No. 39
v_r=0.0124 m/sec, R < 17 mm
(b) Test No. 16
v_r=0.00158 m/sec, 17< R < 24 mm
(c) Test No. 29
v_r=0.0297 cm/sec, 17< R < 24 mm
(d) Test No. 51
v_r=0.00684 cm/sec, 17< R < 24 mm
(e) Test No. 28
v_r=0.0355 cm/sec, R < 17 mm
(f) Test No. 18
v_r=0.11 cm/s, R >24 mm
Normalized mass
Distance downflume (m)

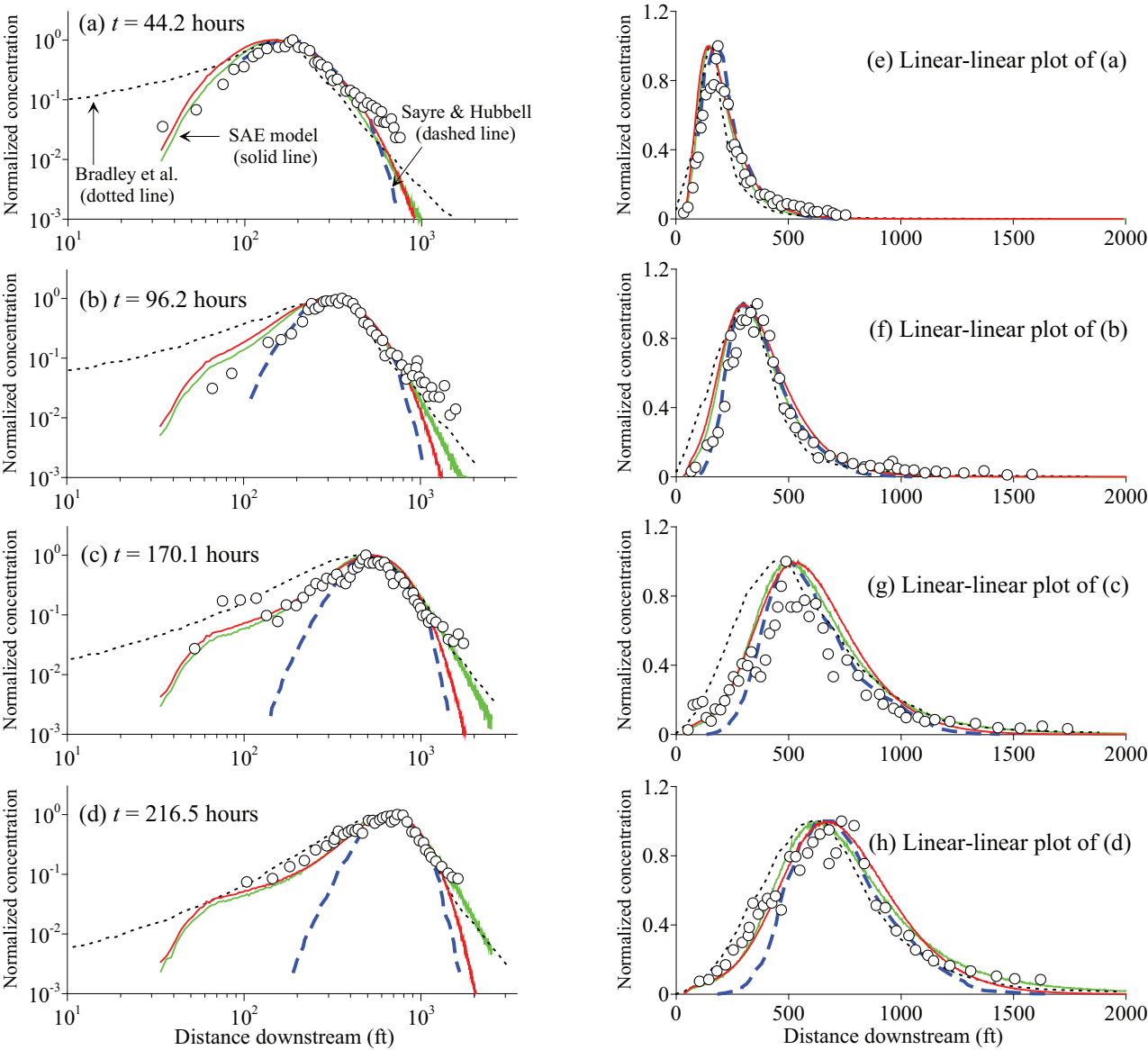
(a) t = 44.2 hours
(b) t = 96.2 hours
(c) t = 170.1 hours
(d) t = 216.5 hours
Normalized concentration
Distance downstream (ft)
Sayre & Hubbell
(dashed line)
SAE model
(solid line)
Bradley et al.
(dotted line)
(e) Linear-linear plot of (a)
(f) Linear-linear plot of (b)
(g) Linear-linear plot of (c)
(h) Linear-linear plot of (d)

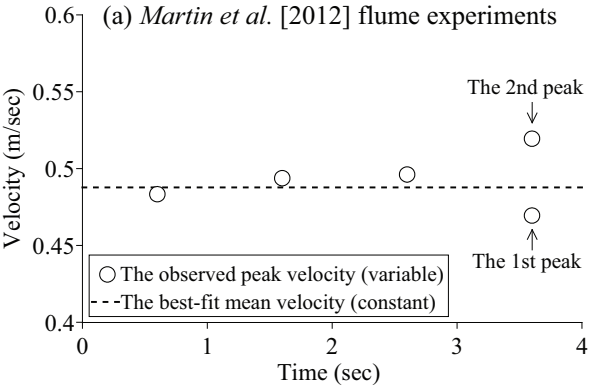
(a) Martin et al. [2012] flume experiments
Velocity (m/sec)
Time (sec)
The 2nd peak
The 1st peak
The observed peak velocity (variable)
The best-fit mean velocity (constant)
0.6
0.55
0.5
0.45
0.4
0
1
2
3
4

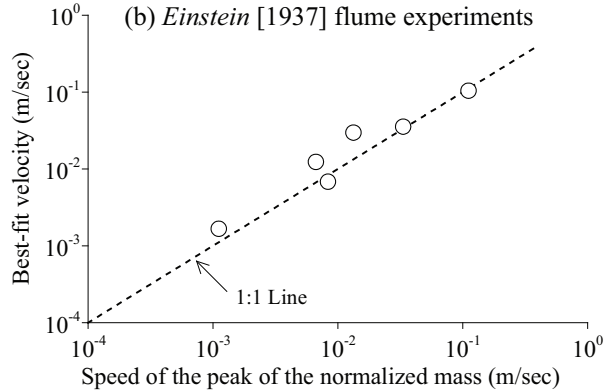
(b) Einstein [1937] flume experiments
Best-fit velocity (m/sec)
Speed of the peak of the normalized mass (m/sec)
1:1 Line
10^0
10^-1
10^-2
10^-3
10^-4

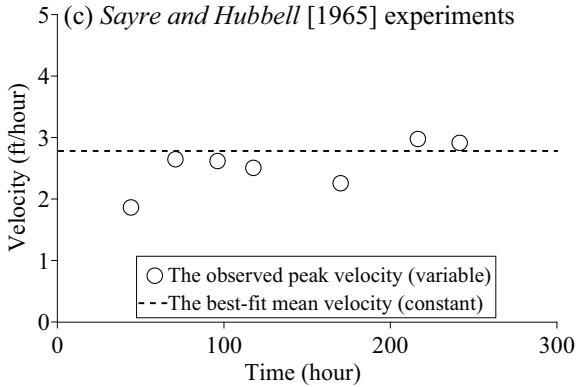
(c) Sayre and Hubbell [1965] experiments
Velocity (ft/hour)
Time (hour)
The observed peak velocity (variable)
The best-fit mean velocity (constant)
5
4
3
2
1
0
0
100
200
300

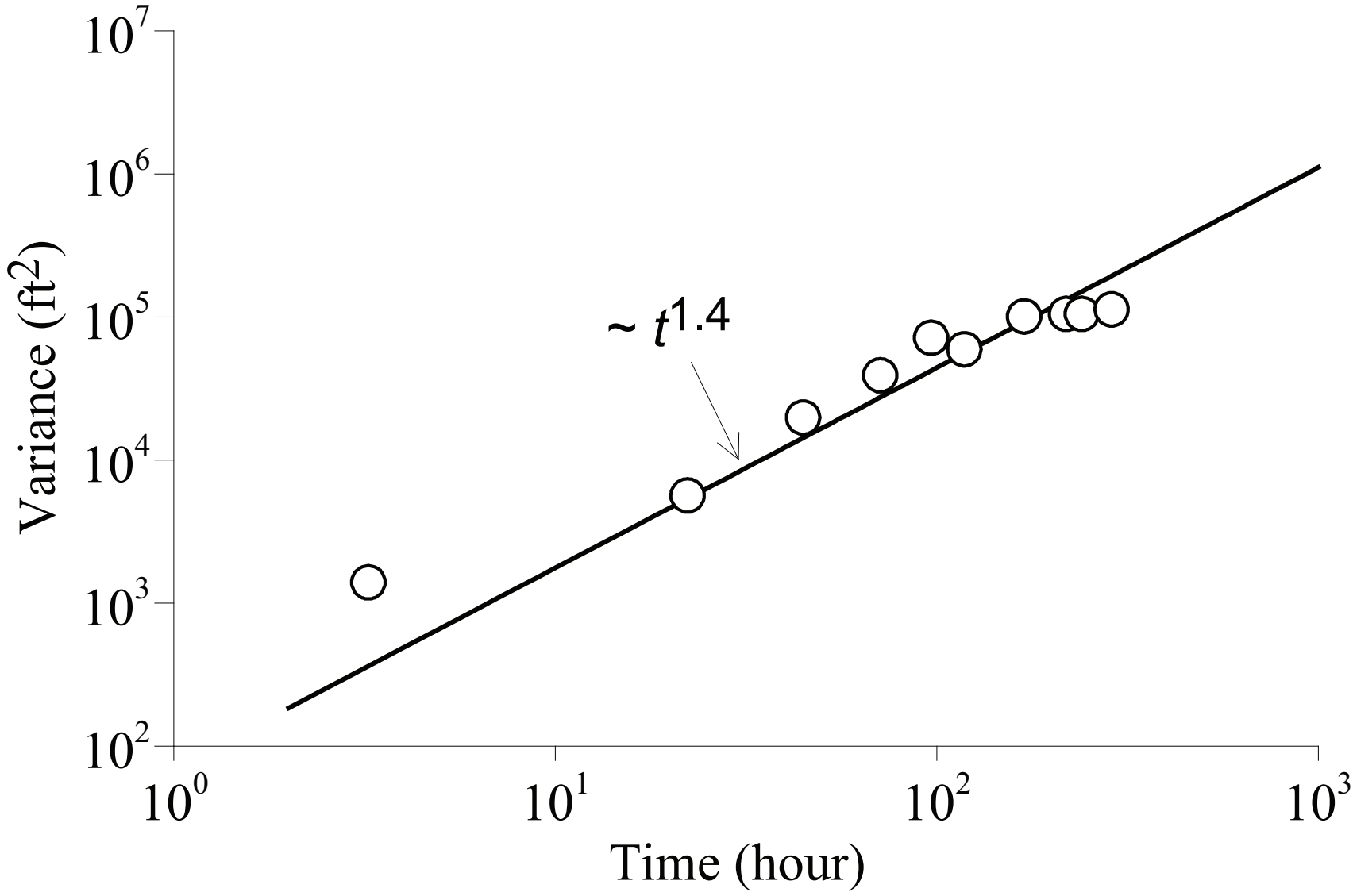
10^7
10^6
10^5
10^4
10^3
10^2
Variance (ft^2)
~ $t^{1.4}$
10^0
10^1
10^2
10^3
Time (hour)

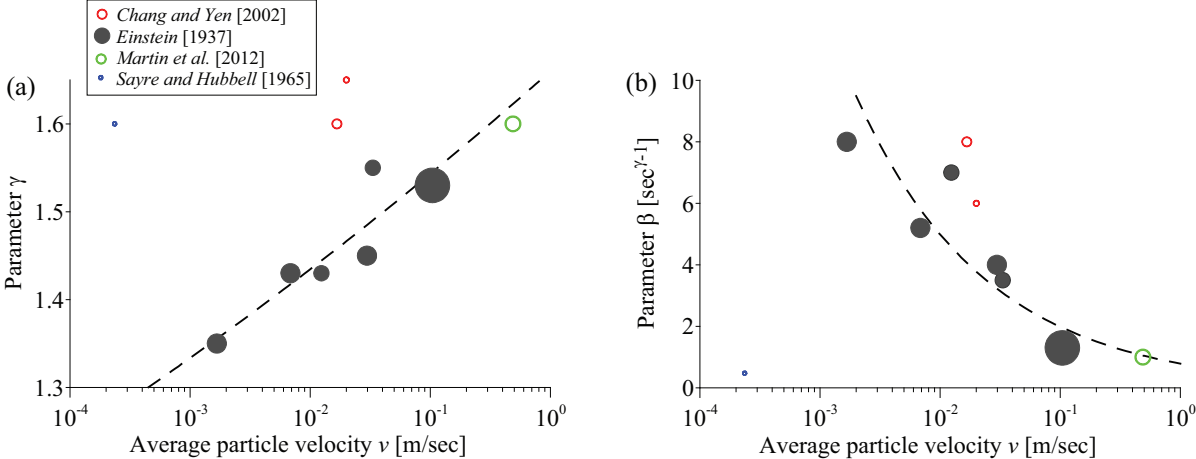
Chang and Yen [2002]
Einstein [1937]
Martin et al. [2012]
Sayre and Hubbell [1965]
(a)
Parameter γ
1.6
1.5
1.4
1.3
10^-4
10^-3
10^-2
10^-1
10^0
Average particle velocity v [m/sec]
(b)
Parameter β [sec^γ-1]
10
8
6
4
2
0
10^-4
10^-3
10^-2
10^-1
10^0
Average particle velocity v [m/sec]

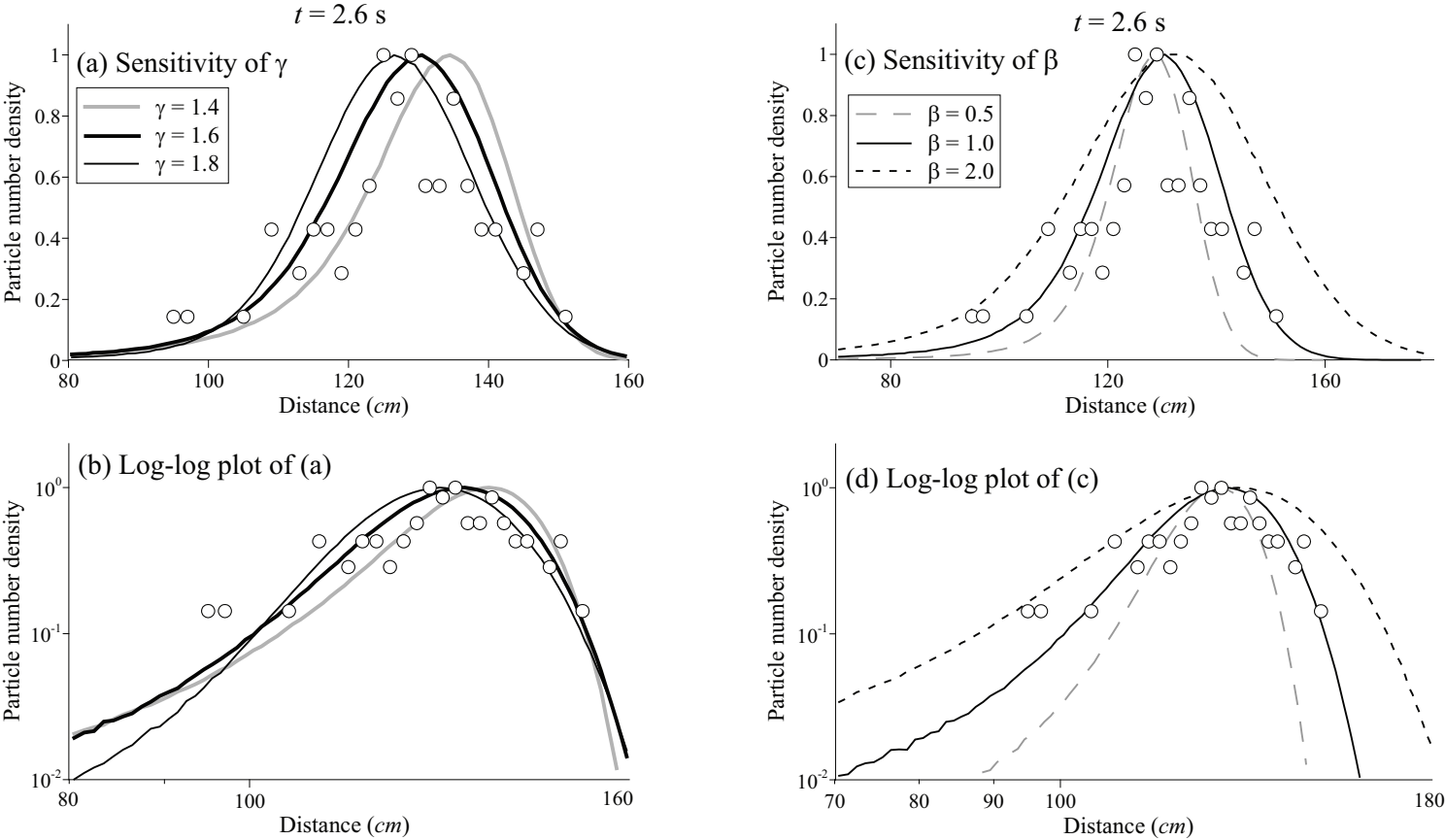
t = 2.6 s
(a) Sensitivity of γ
γ = 1.4
γ = 1.6
γ = 1.8
Particle number density
Distance (cm)
(b) Log-log plot of (a)
Particle number density
Distance (cm)
t = 2.6 s
(c) Sensitivity of β
β = 0.5
β = 1.0
β = 2.0
Particle number density
Distance (cm)
(d) Log-log plot of (c)
Particle number density
Distance (cm)

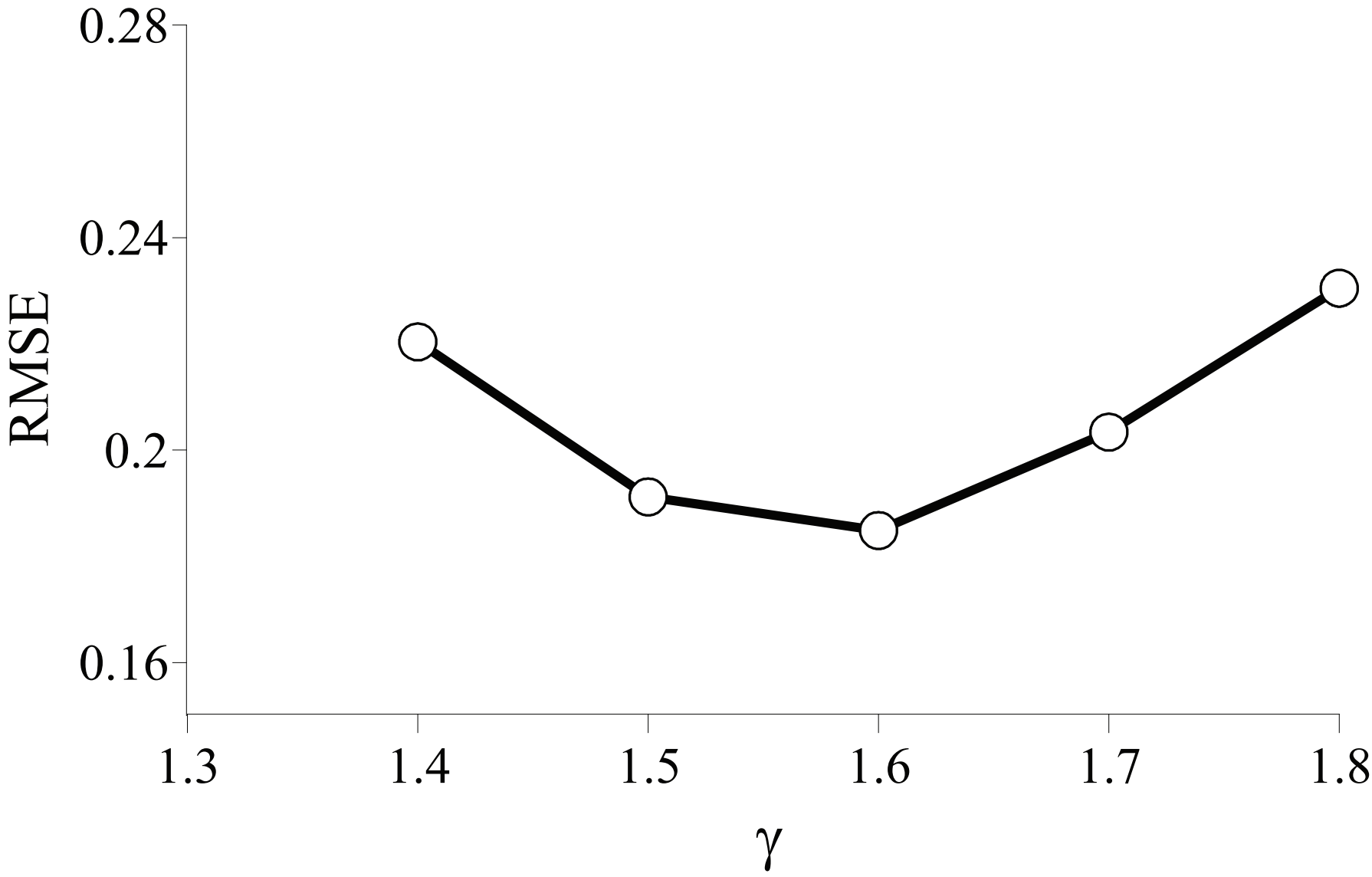
0.28
0.24
0.2
0.16
RMSE
1.3
1.4
1.5
1.6
1.7
1.8
γ

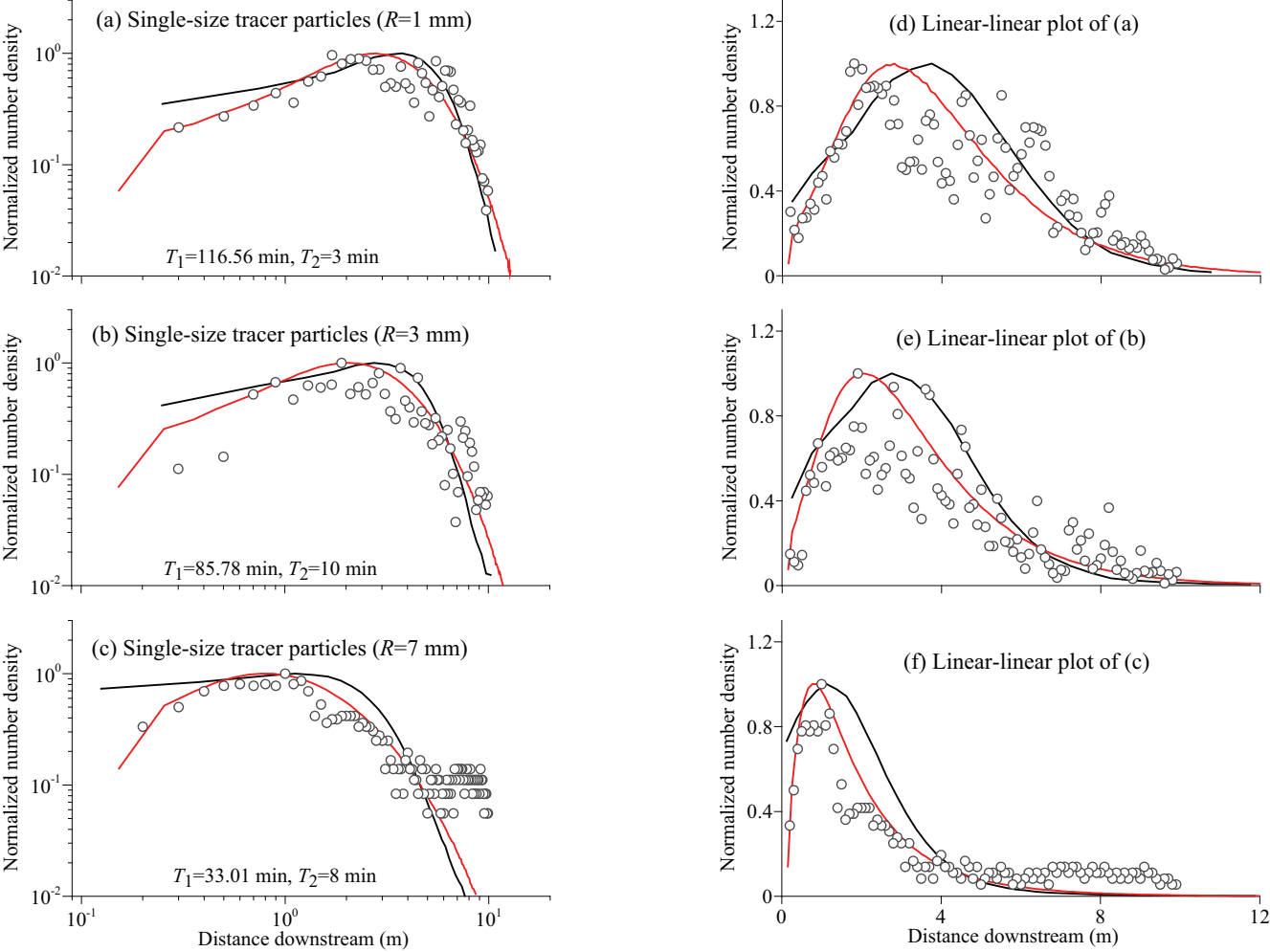
(a) Single-size tracer particles (R=1 mm)
T1=116.56 min, T2=3 min
(b) Single-size tracer particles (R=3 mm)
T1=85.78 min, T2=10 min
(c) Single-size tracer particles (R=7 mm)
T1=33.01 min, T2=8 min
(d) Linear-linear plot of (a)
(e) Linear-linear plot of (b)
(f) Linear-linear plot of (c)
Normalized number density
Distance downstream (m)

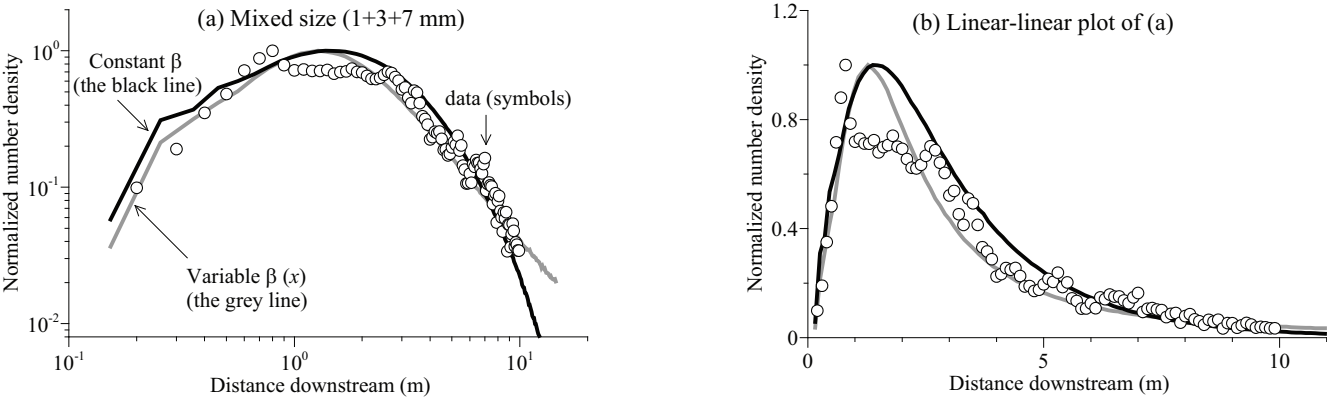
(a) Mixed size (1+3+7 mm)
Constant β
(the black line)
data (symbols)
Variable β (x)
(the grey line)
Normalized number density
Distance downstream (m)
(b) Linear-linear plot of (a)
Normalized number density
Distance downstream (m)